Norwegian University
of Life Sciences

Master's Thesis 2023 30 ECTS
Faculty of Science and Technology

Buckling capacity of axially loaded screws in timber

Martin Steimler
Structural Engineering and Architecture

Acknowledgements

This Master's thesis was written as the culmination of my Master of Science studies in Structural Engineering and Architecture at the Norwegian University of Life Sciences (NMBU). The work in this thesis corresponds to a scope of 30 study credits. The assignment was proposed by Roberto Tomasi and appealed to me due to the topic of pressure perpendicular to the grain. The reinforcement of this concept will be highly useful for me as a structural engineer working with timber, as I frequently encounter this problem. Furthermore, this topic presented an interesting opportunity to participate and gain valuable insight into how European standards are developed and researched.

It has been highly educational and fascinating to work with a topic that is of interest across Europe, from Norway to Italy, and the ongoing work in Germany.

I wish to express my gratitude to all those who have helped me. First and foremost, my tutors Roberto Tomasi, Angelo Aloisio, and Yuri De Santis. You have all provided valuable insights and guidance, for which I am profoundly grateful. For the help with the lab tests, I want to thank Xiaojun Gu and Roar Økseter for their assistance with performing tests and the subsequent work in the lab. Additionally, I am grateful to SFS for providing the screws for the tests.

Last but not least, I want to express the deepest gratitude to my family, Kathrine and Nora, for being patient and supportive throughout the thesis and my education. I look forward to repaying this gesture.

Ås, Mai, 2023

Martin Steimler

Summary

This thesis aims to validate or challenge Alioso et al.'s work on timber screw buckling through experimental and FEM analysis. The effects of inclination and density, not considered in the original study, are also examined.

The laboratory tests utilized screws of 6, 8, and 10 mm diameters with lengths from 100mm to 340mm. Each test involved three screws, tested at angles of 0, 5, and 10 degrees. The density of the timber specimens was also measured. None of the 6 mm screws underwent buckling, thus were not further evaluated. These experiments were then verified using FEM analysis, with the experimental findings being reproduced and compared with the results from the tests. The outcomes of the FEM analysis coincided with the experimental results.

The results of this study demonstrated that the effect of density was far more significant than what was suggested by the calculation model. Similarly, the angle of the screw also had a significant effect on the force the screw could withstand. Given the large variation observed within all sorting parameters, it is reasonable to infer that the materials have the greatest influence. While wood is a material with significant variability, the importance of the steel used in the screw should not be underestimated.

Alioso et al.'s calculation model proves to correspond with experimental tests, specially for the 8 mm tests. However, for the 10 mm screws, there was a deviation in both the experimental tests and FEM analyses. The buckling form for both screw dimensions was as described by Alioso et al. The reason for the 10 mm screws having a lower load capacity remains unclear, but one hypothesis is that it could be due to larger screws having a higher load, leading to greater buckling force. The density tests enabled this hypothesis, as they demonstrated the timber's importance supporting the screw to be more critical than previous calculations have suggested.

This thesis confirms the findings of Alioso et al. Moreover, it highlights a previously underestimated factor and thus a knowledge gap that requires further research to refine the mathematical formulation.

Sammendrag

Denne avhandlingen har som mål å validere Alioso et al.'s nye matematiske tilnærming til knekking av skruer i treverk gjennom eksperimentelle tester og FEM-analyse. Effektene av vinkel og tetthet, som ikke ble vurdert i den opprinnelige studien, undersøkes også.

Laboratorietestene benyttet skruer med diametre på 6, 8 og 10 mm med lengder fra 100 mm til 340 mm. Hver test involverte tre skruer, testet i vinkler på 0, 5 og 10 grader. Densiteten til limtreet ble også målt. Ingen av 6 mm skruene viste tegn til knekking, og ble dermed ikke vurdert videre. Disse eksperimentene ble deretter verifisert ved hjelp av FEM-analyse. Resultatene fra FEM-analysen samsvarte med de eksperimentelle resultatene.

Resultatene fra denne studien viste at effekten av tetthet var langt mer betydelig enn det som ble antydet av tidligere beregningsmodeller. Skruens vinkel hadde også en betydelig effekt på kraften skruen kunne motstå. Gitt den store variasjonen som ble observert innen alle parametre som ble sortert etter, er det rimelig å anta at materialene har størst innflytelse. Selv om tre er et materiale med betydelig variabilitet, bør betydningen av stålet som brukes i skruen ikke undervurderes.

Alioso et al.'s beregningsmodell viser seg å samsvare med eksperimentelle tester, spesielt for 8 mm testene. Imidlertid var det en avvik for 10 mm skruene, både i de eksperimentelle testene og FEM-analysene. Knekkeformen for begge skruedimensjonene var som beskrevet av Alioso et al. Årsaken til at 10 mm skruene hadde lavere knekningslast enn beregningene er ikke bevist. En hypotese er at det kan skyldes at større skruer har en høyere belastning, noe som fører til større knekkingskraft. Densitetsfunnene muliggjør denne hypotesen, da de viste at treverkets betydning for å støtte skruen er mer kritisk enn tidligere beregninger har antydet.

Denne oppgaven bekrefter funnene til Alioso et al. Videre fremhever den en tidligere undervurdert faktor og dermed et kunnskapshull som krever ytterligere forskning for å forbedre den matematiske formuleringen.

Table of Contents

List of Figures

List of Tables

1. Introduction

Recent advancements in the production of engineered wood and efficient adhesives have led to cost-effective production of larger cross-sections and longer spans. This has resulted in a surge of interest in long-span timber structures(12). Furthermore, the height of timber buildings has been steadily increasing, with notable examples including the 85.4-meter-tall Mjøstårnet in Norway, the 53-meter-tall Tall Wood Residence at the University of British Columbia, and the Ascent MKE Building in Wisconsin, which is planned to reach a height of 84 meters. Timber, being a sustainable material with excellent acoustic and thermal properties, is a suitable choice for constructive members(12).

Timber is an anisotropic material, but it is often considered orthotropic in engineering models(13). This means that not only do the properties vary in different directions, but also the direction of applied load affects the strength of the timber. This characteristic enables the creation of long spans, but can also present a challenge when transferring loads from, for example, a beam or truss to a column. The compressive strength of timber perpendicular to the fibers is about 1/8th of the strength parallel to the grain(6). To fully utilize timber in structures, there is a need for effective solutions to handle this challenge. Some of these solutions include increasing the surface area by using a steel plate or enlarging the cross-section, employing doweled connections, or reinforcing with screws. Self-tapping screws have proved to be a cost-effective way of addressing this issue(6).

Several studies have been conducted on the failure of perpendicularly reinforced timber structures, such as those by Haande and Thunberg(3), Bjetka(14), and Nilson(15). Failures in a reinforced timber part may be due to the timber itself or the screws used for reinforcement. The former has been extensively researched, from studies in the 1940s/50s cited in Côté Kollmann(16), to recent studies by Fortino et al.(17) and Müller et al.(2). The latter, screw failure, can be further categorized into push-through failure and buckling failure. While failure in the timber and push-through failure (including pull-out) have been widely researched, there are only two papers published on buckling failure of screws (7)(6). The first of these is based on only a few tests, which underscores the need for further research. As pointed out by Aloisio et al.(7), "The analytical expression for

calculating the buckling load does not follow the observed modes."

1.1 Problem Statement

Despite the common issue of perpendicular compression in timber buildings, and the use of self-tapping screws as one of the few prevalent solutions, there is a limited understanding and research on the topic. The problem can be broken down into two key questions:

- What factors contribute to the increase and decrease of buckling capacity?
- How does the calculation model proposed by Aloisio et al.(7) compare to experimental results?

1.2 Research Objectives

The overarching goal of this research was to contribute to a better understanding of reinforced timber subjected to perpendicular load. This objective was then divided into two specific aims:

The first aim of this thesis is to investigate the buckling of screws in timber using a blend of experimental tests and numerical analysis. As mentioned earlier, there have been only two prior studies that have delved into this subject (7)(6), neither of which employed a 3D model. The experimental research carried out in this thesis will also contribute to one of the largest number of tests on this subject. As a result, the second aim of this research is to bridge the knowledge gap in this field by enhancing scientific understanding of screw deformation and pinpointing the most critical parameters that determine maximum load capacity. The final aim will be to analyze how the new model proposed by Aloisio et al.(7) compares to the findings from the experimental tests, and, if possible, contribute to further optimization of the model.

1.3 The Process

Given the active nature of this research area, the initial focus of the thesis, which centered on the numerical analysis of reinforced timber subjected to perpendicular pressure, has evolved over the course of the project. Although the results from the numerical analysis were reasonably accurate regarding maximum load, buckling was not considered. As a result, the latter half of the thesis shifted objectives, ultimately leading to the two previously stated aims: conducting experimental tests followed by a numerical analysis on axially loaded screws buckling in timber.The initial research will be presented and described to some degree, as it forms part of the process and to some extent corroborates the initial numerical studies.

1.4 Limitations

The following assumptions, limitations, and simplifications are made:

- The numerical study is somewhat limited by the fact that the author has not previously studied non-linear finite element methods, nor used Abaqus.
- The glue is not considered in either the numerical or experimental tests.
- The screw head is not considered in the numerical model.

2. Theory

2.1 Timber

The trunk of a tree consists of millions of individual woody cells, that vary both in length and width, normally much longer than wide. Most of these cells are arranged in the same direction, called the longitudinal direction.(16, p. 2) The two other directions in timber is radial and tangential. Lignin is "gluing" the cells together, as well as providing stiffness to the cell walls.(1, p. 234)These cells are then “glued” together with lignin. For species like spruce and pine, from now on referred to as timber, cells are arranged into early and late wood as seen in the figure 2.1 from Müller et al. (2)

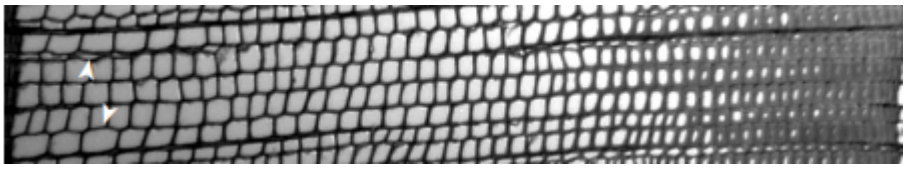

Figure 2.1: Arrangement of cells in growth ring

A wooden cell is built up as illustrated in figure 2.2 For this topic, pressure perpendicular, the space in the middle, lumen, is a limiting factor. The cell walls starts to collapse when the pressure causes buckling in the cell wall(2). High density timber has in general higher capacity, due to having smaller lumen than fast growing light timber. Within a tree early wood grows faster than late wood and normally has larger lumen, as visualized in figure 2.1 This causes the early wood to collapse first as seen in figure 2.3

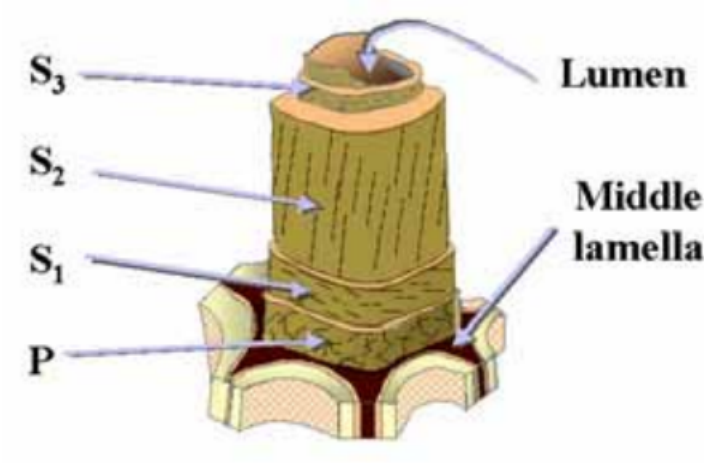

Figure 2.2: Wood cell(1)

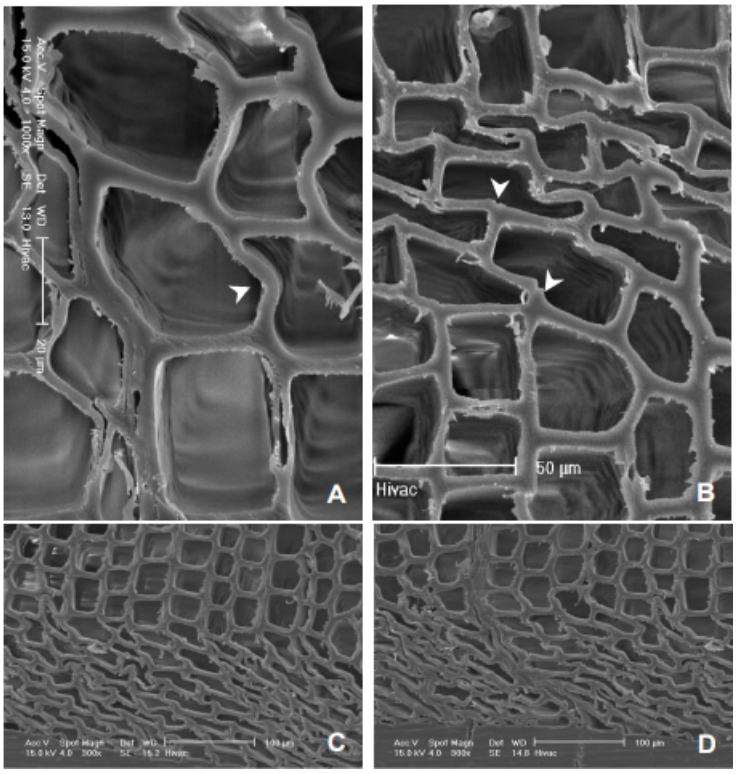

Figure 2.3: Cell walls collapsing (2)

Müller et al.(2) did a buckling calculation for cells using Euler buckling. Where the calculations coincided with the pressure tests. Both with regards to when deformation started and maximum load. The early wood with largest lumen collapsed first and late wood last as discussed previously.

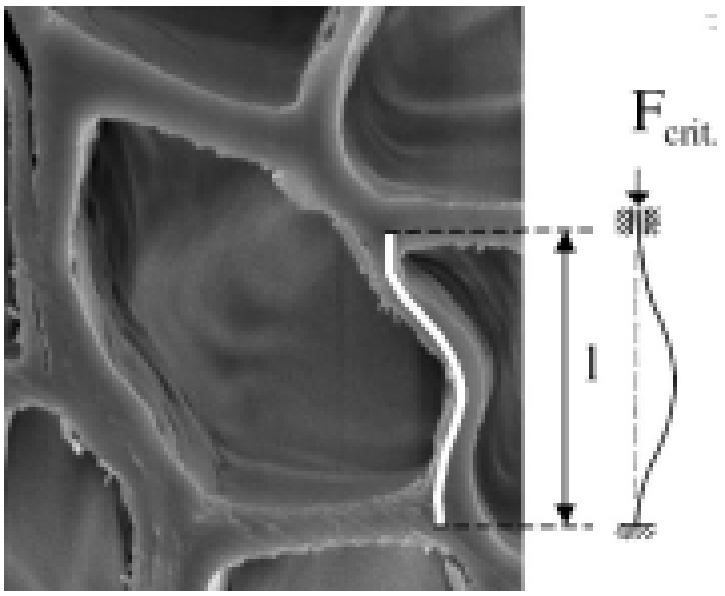

Figure 2.4: Buckling of the cell wall(2)

Fibre saturation is also another factor affecting the strength of the timber. According to Côté & Kollmann this is due to the water molecules being deposited between the micelles and thus increasing the distances between them. Which in turn causes a reduction of the intermicellar attractive forces and therefore of the cohesion. (16, p. 349).

The behavior of timber compressed perpendicular to the grain can be divided into elastic and plastic deformation. A material is within the elastic range when it is capable to recover to its original shape after deforming due to load, and the stress strain relationship is linear. When the material is no longer able to recover back to it‘s original shape its considered to be in the plastic range, until fracture is reached. For compression perpendicular this means that the elastic range is up til the load where the first cell collapses. Timber has an elastic-plastic behaviour. There is no clearly defined ultimate stress for compression perpendicular to grain, where the material is assumed to be infinitely stiff under the condition of compression perpendicular to grain (3) (18, p. 67-70). As displayed in graph 2.5 from Haande and Thunberg (3) .

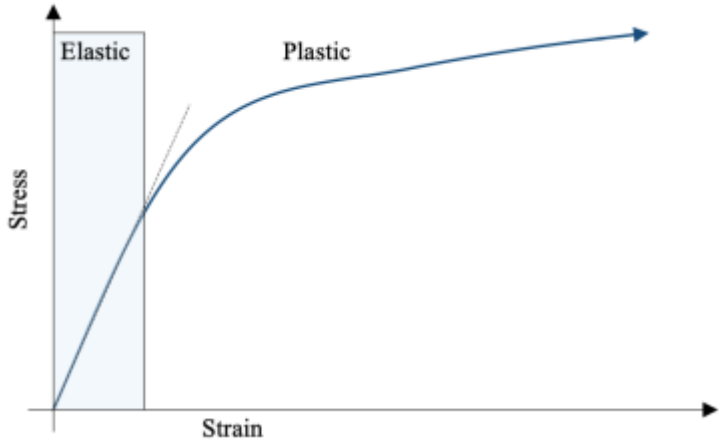

Figure 2.5: Stress strain curve(3)

2.2 Abaqus

Abaqus is a finite element software developed by Dassault Systèmes Simulia Corp(19), designed for various applications, including calculating the mechanical strength of components.

The Abaqus software employs the finite element method (FEM). FEM is a systematic procedure of approximating continuous functions as discrete models. This is done by breaking the model into smaller parts, called elements. The elements are connected to points called nodes. The nodes are again connected to other nodes. By doing this a mesh is created over the entire shape. Each of the elements then holds a local approximation of the problem at hand based on the values at its nodes. The accuracy depends on how fine the mesh is, as finer mesh gives a more precise answer. However, at some point the results will converge, and the solution approaches the correct answer(20).

There are two major ways of utilizing Abaqus in a problem like the one presented in this thesis. The implicit solution method finds unknown values by iterating the

unknown quantities, meaning that each increment must converge, making the process computationally expensive. However, the size of the time increment does not limit the solution, resulting in an unconditionally stable method requiring fewer increments for analysis completion. This method is ideal for problems with long response times and relatively small non-linearities (21).

Conversely, the explicit method determines unknown values based on already known quantities, eliminating the need for iteration and offering a time-saving analysis. Unlike the implicit method, convergence is not a problem, but the analysis requires both small and numerous time increments. The size of the time increment is proportional to the size of the smallest element in the model. Consequently, small elements around areas like screw holes result in smaller increments. The explicit method is generally preferable for quasi-static problems with large non-linearities and significant contact forces. This is particularly relevant for experiments in this task, involving substantial deformations and contact. To simulate large plastic deformations, the explicit solution method is the preferred choice (21).

When simulating anisotropic yield/creep behavior, such as in loaded timber, Abaqus employs Hill's potential function. This function is an extension of the von Mises yield criterion, adapted to account for material anisotropy. In terms of rectangular Cartesian stress components, the function can be expressed as shown in equation 2.1. All equations in this section is from ABAQUS Analysis User's Manual (22).

$$f(\sigma) = \sqrt{F(\sigma_{22} - \sigma_{33})^2 + G(\sigma_{33} - \sigma_{11})^2 + H(\sigma_{11} - \sigma_{22})^2 + L\sigma_{23}^2 + 2M\sigma_{31}^2 + 2N\sigma_{12}^2} \tag{2.1}$$

In order to calculate the input parameters in Abaqus, the material parameters must be known. Firstly, the R values (R1, R2, and R3) must be determined using these formulas for R_{nn} that are as follows $R_{11} = \frac{\bar{\sigma}11}{\sigma^0}$, $R_{22} = \frac{\bar{\sigma}22}{\sigma^0}$, $R_{33} = \frac{\bar{\sigma}_{33}}{\sigma^0}$, $R_{12} = \frac{\bar{\sigma}_{12}}{\tau^\circ}$, $R_{13} = \frac{\bar{\sigma}_{13}}{\tau^\circ}$ and $R_{23} = \frac{\bar{\sigma}_{23}}{\tau^\circ}$. These values obtained from these calculations provide anisotropic yield stress ratios (22). In simpler terms the ratios takes into account the ratios for the material's non-linear response across various directions.

After calculating the R values, values for F, G, H, L, M, and N are calculated as follows in equations 2.2 to 2.7:

$$F = \frac{1}{2}\left(\frac{1}{R_{22}^2} + \frac{1}{R_{33}^2} - \frac{1}{R_{11}^2}\right) \tag{2.2}$$

$$G = \frac{1}{2}\left(\frac{1}{R_{33}^2} + \frac{1}{R_{11}^2} - \frac{1}{R_{22}^2}\right) \tag{2.3}$$

$$H = \frac{1}{2}\left(\frac{1}{R_{11}^2} + \frac{1}{R_{22}^2} - \frac{1}{R_{33}^2}\right) \tag{2.4}$$

$$L = \frac{3}{2}R_{23}^2 \tag{2.5}$$

$$M = \frac{3}{2}R_{31}^2 \tag{2.6}$$

$$N = \frac{3}{2}R_{12}^2 \tag{2.7}$$

In order to calculate linear buckling, Abaqus has a "Buckling step". This step utilizes a linear perturbation procedure, which in short means linearizing the equations and assuming small displacements and rotations. One may include preloads (P^N) in the analysis; however, in classical eigenvalue buckling analyses, it's normal to only define incremental loading (Q^N) in the buckling prediction step (23). The magnitude applied is of little interest as it gets scaled by the calculated load multiplication factor (λ_i) that is calculated in the eigenvalue problem. Finally, the buckling load is given as the multiplying factor of the load the user of the program applied ($\lambda_i Q^N$) and if preload is added, $\lambda_i Q^N + P^N$. "Buckling step" predicts the theoretical buckling strength of a structure which is idealized as elastic, which may provide higher buckling strength than the experimental values or nonlinear analyses(24). The buckling mode shapes (eigenvectors) are also predicted (25). In this thesis, the second buckling mode, and thus, the second load was of most interest.

The formulation is defined as follows in ABAQUS Analysis User's Manual (25):

$$(K_0^{NM} + \lambda_i K_{\triangle}^{NM})v_i^M = 0 \tag{2.8}$$

Where K_0^{NM} is the stiffness matrix for the base state (may include preloads). $K_{\triangle}^{NM}$ is a matrix containing the load stiffness due to incremental loading. λ_i is the eigenvalue(s). M and N are degrees of freedom for the whole model. i is the number of the buckling mode (25).

2.3 Self tapping screws

This section describes both the manufacturing process and, and in turn the material properties of the screws as these two are linked to each other. Lastly the shape and cross-section is described. As there are few scientific papers released on this topic this section is largely based on Ringhofer‘s "Axially Loaded Self-Tapping Screws in Solid Timber and Laminated Timber Products" (4). The facts are verified using various sources with differing levels of credibility. High-quality sources, such as authoritative publications and databases like SNL, have been utilized to ensure accuracy and reliability. Additionally, some information has been gathered from sources with comparatively lower credibility, such as manufacturers of similar products. While the latter provided guidance and insight, it may be biased, and therefore it is not cited.

2.3.1 Manufactering process and steel

The raw material used should have properties suited these processes. Thus steel denoted as "cold extrusion steels" are most suitable given in ON-EN/NS-EN 10263-4. The steel types are in general low alloy carbon steels (4). This steel is then used in the following manufacturing process, which is divided into five steps(4):

- Properties and pre-treatment of raw material
- Forming the screw geometry
- Screw hardening process
- Adding protective coats
- Final treatment

Fort this study the first three points is the most important as they decide the mecanical strength.

According to Ringhofer (4, p. 123-126) self-tapping screws are made of steel wire rods cold formed. Meaning that a screw is made from a rod with the threads pressed inn, thus the screw shank gets a smaller diameter as seen in figure 2.6 (4). For instance the 8mm (thread diameter) Heco topix screws used in this thesis is made from a 5.8mm rod has a shank with a final thread diameter of 5.2mm.

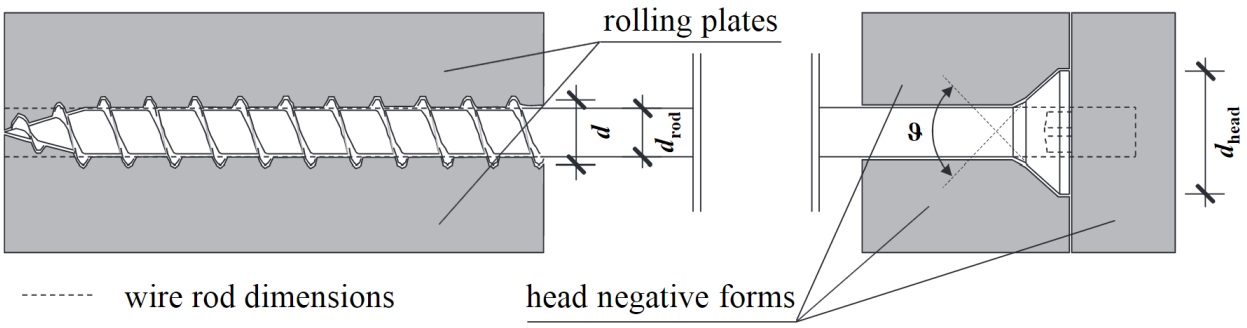

Figure 2.6: Cold-forming process(4)

There are advantages and disadvantages with cold forming. There are two major advantages, were the first is that it lead to an increase of steel hardness, subsequently leading to higher strength. And the other being that it is a cost effective way of manufacturing screws.(4). On the down side, there are two negatives. Were the first being that the previous mentioned hardening of steel leads to lower viscosity and formability, and the latter being unintended dents in the steel that may cause a week point on the screw. If the rolling dies has a defect this will be apparent on every screw at the same place.

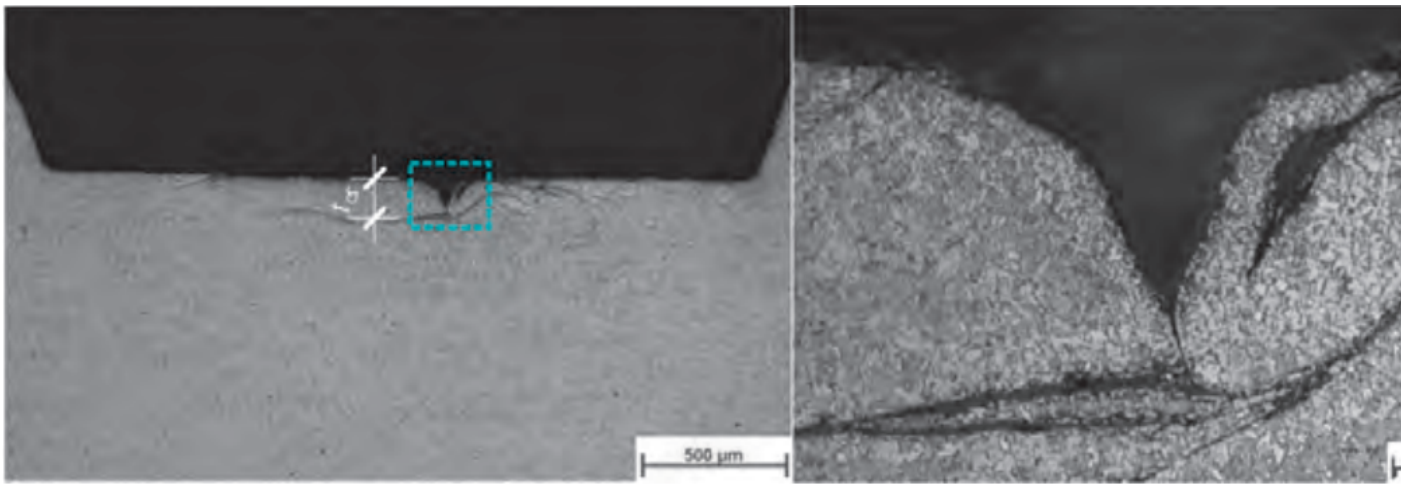

Figure 2.7: "Micrographs (etched) of a self-tapping screw's threaded part related to product group"

The shape of the screw is of major importance. Buckling, as seen above, may be affected by variability in the cross section. Ringhofer (4) (Chapter 3-4) researched the cross-sectional properties of threaded screws. Although the research did not extend to the topic of buckling, there are one major point to take out of the study. The difference between moment of inertia (I) with and without threads, as displayed in figure 2.8 was about 0.25% when comparing the screw shank alone and the screw including the threads for a typical self tapping timber screw. As moment of inertia is one of the main variables when calculating buckling its important to note that the difference is negligible.

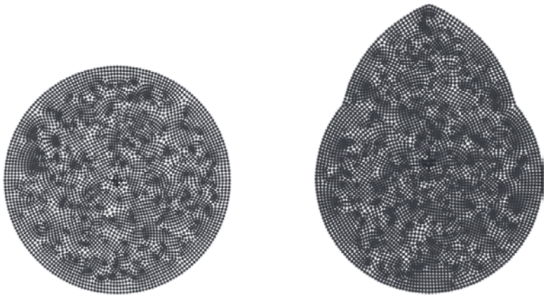

Figure 2.8: The compared sections(4)

2.3.2 Hardening

The hardening process increases the tensile strength of the screw significantly and is a process that different manufactures does in different ways(4). Ringhofer(4) cites Maydl and Tritthart(source unavailable) on the main principle of hardening, witch in turn corresponds the article written by to Almar-Næss(26). Hardening normally consists of four phases described below and visualized in figure 2.9:

- Warm - Warming up to around 900° C
- Austeniting - Warmed material stays under constant temperatur for a certain period of time.
- Quenching - Rapid cooling below 300° C
- Tempering - Warming up between 250-650° C

In the first two phases the steel is heated to around 900° C. At this temperature steel will exist as austenite. Meaning the structure becomes a face-centered cubic structure, where carbon atoms are distributed between the iron atoms in octahedral positions, which provide the most space(26). The cooling phase, called quenching, the crystal structure changes from austenite to martensite. A tetragonal face-centered variant, where carbon atoms are located between the iron atoms and force them apart. Meaning the carbon atoms is between the iron atoms, causing inner lattice stress and thus to increased

strength and hardness, but also makes the steel brittle(26)(4). In the tempering phase the aim is to soften the steel by tempering the steel. This is to some degree reversing the positive effects of the first part of hardening, but on the flip side the ductility increases.

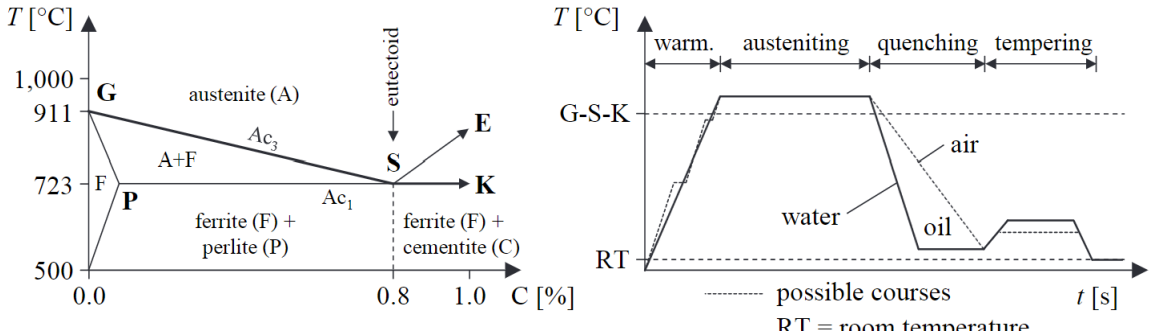

Figure 2.9: Hardening(5)in ringhofer

3. Literature study

3.1 EN 1995-1-1 and ETA

The current method is here presented shortly, as is will be referenced later when discussing previous work on the field. The ETA(27) and EN 1995-1-1 is assumed to share the same formulation. In the ETA formula 3.5 is not multiplied by 2, coincide with the draft of EC5(7).

Calculations is defined as follows:

$$F_{ax,R_d} = k_c \cdot N_{pl,d} \tag{3.1}$$

$$k_c = \frac{1}{k + \sqrt{k^2 - \overline{\lambda}_k^2}} \tag{3.2}$$

$$k = 0.5 \cdot (1 + a_g \cdot (\overline{\lambda} - 0.2) + \overline{\lambda}_k^2) \qquad a_g = 0.49 \text{ prEN 1995-1-1} \tag{3.3}$$

$$\overline{\lambda} = \sqrt{\frac{N_{pl}}{N_{ki}}} \tag{3.4}$$

$$N_{ki} = 2\sqrt{c_h \cdot E_s \cdot I_s} \tag{3.5}$$

$$N_{pl} = \pi * \frac{\pi}{4} * f_y \tag{3.6}$$

$$c_h = (0.19 + 0.012 \cdot d) \cdot \rho_k \cdot \left(\frac{90° + \alpha}{180°}\right) \tag{3.7}$$

Where $E_s = 210{,}000\,\mathrm{N/mm^2}$ and $I_s = \frac{\pi \cdot d_1^4}{64}$.

3.2 Bjetka and Blaß

Bjetka wrote his doctoral thesis on self-tapping screws, which included a chapter on the buckling of screws (14). The thesis was later divided into several papers and conference papers, with Blaß as a co-author(6) in some of them. However, the data used in these papers is based on the initial thesis. In this section, all the previously mentioned articles and the thesis will be referred to collectively.

The investigation done by Bjetka and Blaß was based on experimental tests both in axial and perpendicular direction. The axial test was done with withdrawal tests finding the 3.9 value. The 3.8 perpendicular tests was done as showed in figure 3.1. Were the timber is pushed down on the screw, whom is placed up on steel supports close to the supports. This was done in order to estimate the C_h.

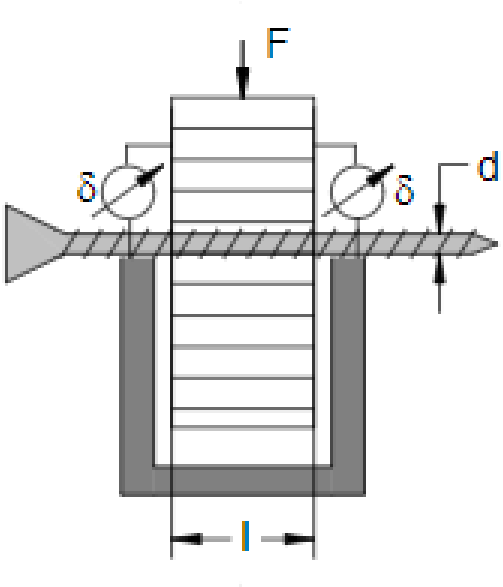

Figure 3.1: C_h test set up (6)

The numerical model was then based on the formulas 3.8 and 3.9 that were deduced form the previously mentioned tests. C_h is the supporting pressure dependent on the angular direction to the grain in the plane. Whilst C_v is the support in the axial direction.

$$c_h = \frac{(0.22 + 0.014d) * \rho}{1.17 \sin^2 \alpha + \cos^2 \alpha} \tag{3.8}$$

$$c_v = 234 * \frac{(\rho * d)^{0.2}}{l_s^{0.6}} \tag{3.9}$$

The model was as displayed in figure 3.2. Where the C_h was put equal to 90° (perpendicular to grain) so the support was as small as possible. The C_v is placed along the screw length, so that the load increases from the screw tip to the screw head when the load is applied. Further they assumed that the screw head was hinged when using a steel plate, unless the screw heads was countersink into the steel plate.

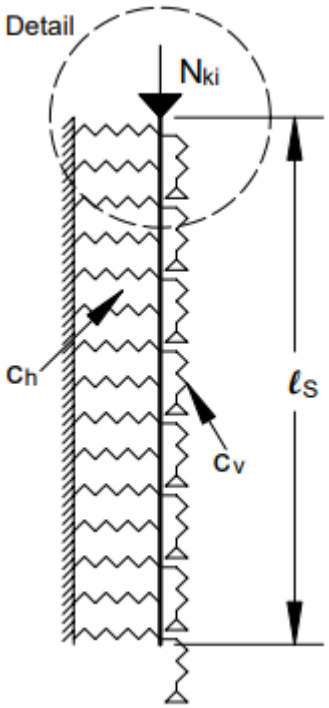

Figure 3.2: Bejtka and Blaß buckling model (6)

3.3 Aloisio et al

The paper writtebn by Aloisio et al.(7) is based on the experimental results of Haande and Thunberg(3), and the formulas provided for C_h and C_v from Bjetka and Blaß(6). The main focus of the paper is creating a expression the theoretical buckling loads in accordance to the observed buckling modes.

- The deformed shape is a simple sine, which does not correspond to the mode of a screw in an elastic medium. A damped sine is more appropriate.
- The formulation does not take into account the boundary conditions for a pinned-pinned beam in equation 3.5. Equation 3.10 is their proposal for theoretical elastic buckling of a Winkler beam.
- The current formula assumes a constant axial force, and the axial stiffness is assumed to be infinite.
- Calibration of the geometric uncertainty factors (a_g) in equation 3.3. Their proposal is $a_g = 0.16$

$$N_{pl} = 2\sqrt{c_h EI}\frac{\sqrt{5 + 6\pi^2 + \pi^4}}{1 + \pi^2} \approx 1.17 N_k \tag{3.10}$$

The authors applied a method similar to Bjetka's with regards to springs. However, for their linear analysis, the calculations for c_h followed EN 1995-1-1, using equation 3.6. The c_v value was calculated using the same formula, equation 3.9. The head was restrained from transverse displacements but allowed to rotate. Unlike in Bjetka's approach, as the authors pointed out, the screw head was considered pinned, as seen in the left model of figure 3.3. The diameter was set as $1.1d_1$. A linear elastic constitutive model was adopted for steel ($E = 210,000, N/mm^2$). The non-linear approach was quite similar, but the steel modeling was elastic-plastic.

An imposed displacement was applied to the head on a defected screw geometry, obtained from the linear buckling model, as seen in the right model of figure 3.3.

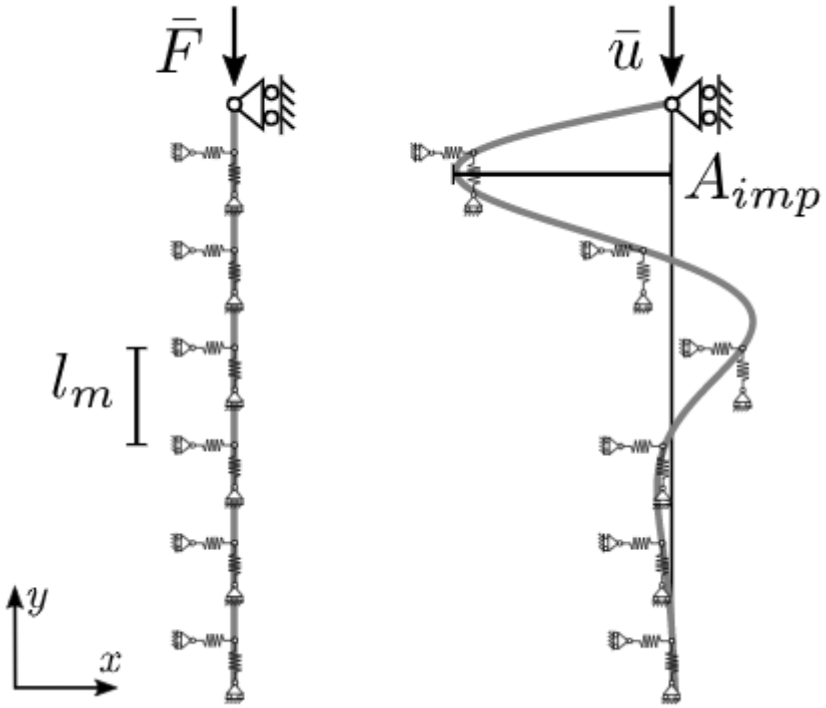

Figure 3.3: Finite element models Aloisio et al.(7)

4. Methods

4.1 Abaqus

As previously mentioned, the numerical campaign started by replicating the test done by Haande and Thunberg(3). The numerical buckling study was largly bases on the same asumptions and modeling. Thus, this section presents the modeling and asumptions done in the initial model, whilst presenting the buckling model. The differences will be pointed out and described.

The modeling assumptions with regards to modeling solutions and input for the models in Abaqus were based mainly on De Santis et al.(8), but also on Avez et al(28) and Bendon et al(29). The model consisted of three parts: the screw shank, a fictitious "soft-layer," and the timber. This meant that the screw was divided into shank and threads combined with perforated timber, modeled as a steel rod with a surrounding cylinder made out of a perfectly elastic soft-layer, as seen in Figure 4.1, described in its own section. Since the screw and soft-layer were modeled as one part, the two parts would not glide or separate. The connection between the soft layer and timber is, however, described by an "Interaction property" discussed in a separate section.

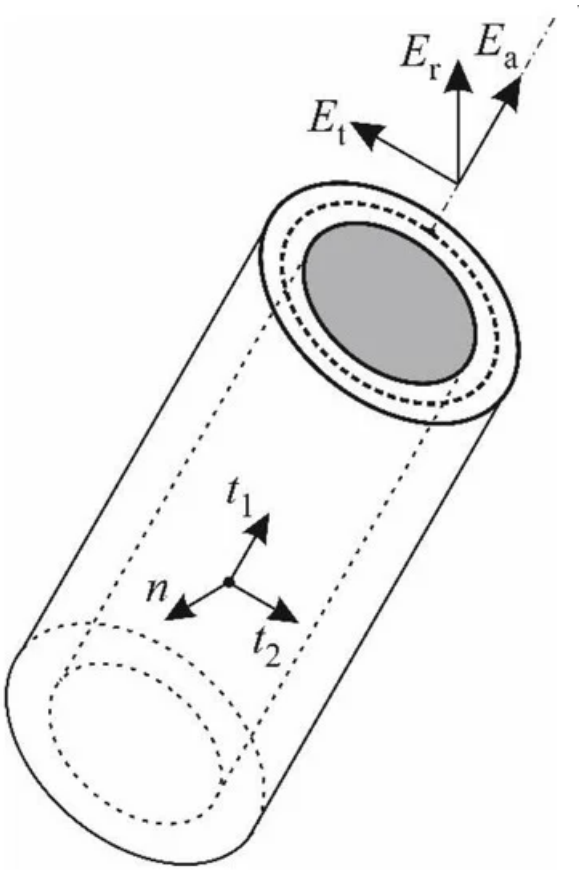

Figure 4.1: Screw and soft-layer with cohesive contact geometries and reference system (8)

4.1.1 Screw

The screw shank, the gray section in figure4.1, is made out of carbon steel and modeled as an elastic-plastic material with elastic modolus $E_s = 210,000 N/mm^2$ as De Saints et al.(8) did. With a f_y of $900 N/mm^2$ according to ETA-19/0553 (27).

4.1.2 Soft-layer

Due to the fact that the soft layer is fictitious both the material parameters of the layer and the interaction property not possible to measure. Thus, it the material properties is adjusted by trial an error until the wanted behaviour is attained. The starting point for these values came from the work done by De Saints et al.(8), En 1408 and EN 338. However, as previously mentioned the doctoral thesis by by Bejtka (14) has equations for C_v and C_h displayed in equations 3.8 and 3.9. The values for the soft-layer is displayed in table 4.1.

		Final models		
Property	Initial model	Low density	Medium density	High density
E1	300	151	160	175
E2	300	128	140	148
E3	300	300	300	300
Nu12	0	0	0	0
Nu13	0	0	0	0
Nu23	0	0	0	0
G12	610	650	650	650
G13	610	650	650	650
G23	610	650	650	650

Table 4.1: Softlayer properties

4.1.3 Contact properties

The contact between the soft layer and the timber was defined by trial and error as previously described. The testing confirmed that the best results were obtained using the following contact properties options: Tangential behavior with friction of 0.5, to reproduce the post-failure behavior. After reaching the maximum stress on the cohesive surface, the screw penetrates the timber with friction being the only residual resisting mechanism. Normal behavior with "hard contact". Cohesive behavior Knn=0 and Kss=Ktt=15. Damage, which had the greatest influence on the results, had the following input "Normal only" = 0.1, "Shear-1 only" = 8 and "Shear-2 only" = 8. The normal-only values have been decided with trial and error based on tests and the mean value of those numbers.

4.1.4 Timber

Material properties for timber, displayed in table 4.2, are mostly mean values from EN 384:2016 and EN 14080:2013. This was done both as a simplification of the model and as a means to get a model using the properties from the Eurocodes, making it as statistically equal to the mean value of the tests as possible. Due to using combined glue-laminated timber, the material properties varied throughout the section. GL30c, as was used, is from Moelven Limtre AS and consists of T22 and T14. The distribution in the test elements was 1/6 of the height from the bottom and tom consisted of T22 and the middle part of T14 class timber. The Poisson's ratios for timber were not particularly important in the model due to the fact that the forces from this were of secondary effect and are in fact set to 0 by Avez et al(28) when creating a similar model. The ratio of 0.4 was used due to the fact that the model was simplified, as the material parameters were too, and it is quite close to the actual values. The values are stated in radial, tangential, and longitudinal directions as in Côté & Kollmann(16) but this does not coincide with the directions used in Eurocodes were the material parameters for the model was extracted form. It must also be mentioned that the glue layer between the lamellas is neglected. Hardeng(30) tested this when doing a similar study and concluded that the glue had an effect on deformation. However, the properties of the glued interaction were not accessible.

	Initial model		Final model				
Property	T22	T14	T16	T26	T30	Unit	Soure
E1	1300	1100	11500	14000	15500	MPa	384:2016/EN338:2016
E2	430	370	380	470	520	MPa	384:2016/EN338:2016
E3	430	370	380	470	520	MPa	384:2016/EN338:2016
Nu12	0.4	0.4	0.4	0.4	0.4		(16)
Nu13	0.4	0.4	0.4	0.4	0.4		(16)
Nu23	0.4	0.4	0.4	0.4	0.4		(16)
G12	812.15	690	720	880	970	MPa	384:2016/EN338:2016
G13	812.15	690	720	880	970	MPa	384:2016/EN338:2016
G23	65	65	65	65	65	MPa	EN 14080:2013 Table 6
Yield stress	37.5	37.5	37.5	37.5	37.5	MPa	(8)

Table 4.2: Timber properties in Abaqus

4.1.5 Mesh

The mesh was produced first and foremost with geometry in mind in order to avoid sharp edges causing singularities. Secondly, the mesh size was decided by approximation, and was at a size where the results converged. The size was also proved to be in about the same size as similar studies(21). The mesh for the majority of the structure is simply made by global seed size of 5. The screw and the region around, as displayed in Figure 4.2, is made with 6 seeds on circular edges. Straight edges have a seed bias of 3 and between 2-4 seeds.

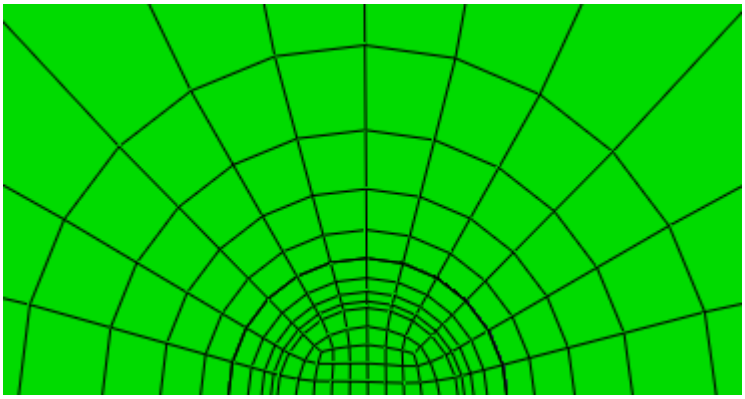

Figure 4.2: Mesh screw

4.1.6 Final model

The final model was largely created using the method described above, with a few changes. The timber part in the final numerical campaign was modeled only as the outer layers of the combined glue-laminated timber. This was done because the properties of timber in the lower lamellas were of lesser interest. The main focus of the final model was on buckling, so the interaction between timber and screw was of less concern in the lower lamellas, as buckling was expected to occur in the upper lamellas. The T-classes are displayed in Table 4.2 in the tests. For the soft layer, the properties were adjusted according to density following the formulas provided by Bjetka, Equations 3.8 and 3.9. The properties of the soft layer are displayed in Table 4.1.

The geometry, as displayed in figure 4.3, was based on the fact that one may assume symmetry, and thus it was reasonable to divide the test in two and only run simulations on half. The red layer is the soft layer, whilst the inner part is the screw shank and the outer part is the timber.

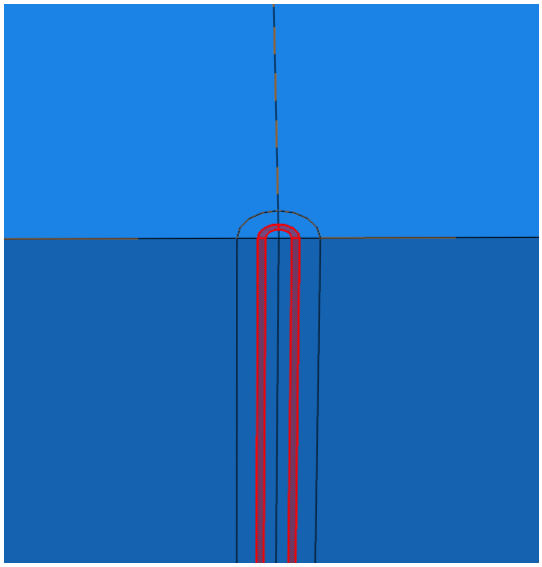

Figure 4.3: Final geometry

The inclination models used medium timber. The challenging part for these models was creating a decent mesh. After several attempts without success in creating a suitable mesh, the problem was reconsidered. A simpler yet fully satisfying solution was to tilt the element the desired degrees, but assign the material properties in global coordinates. This enabled the use of a standard mesh. Although the geometry was somewhat off, it did not affect the buckling strength, as the distance to the end was still large enough that this did not pose a problem.

4.1.7 Buckling step

For the final tests, Abaqus's buckling step was used. The model was in large parts the same as the previous description. The interaction properties, however, had to be suppressed and replaced with a tie constraint between the screw surface and timber surface.

4.1.8 Extracting results

Extracting results proved to be somewhat challenging. As the screw geometry was smooth and the soft-layer had to be softer than the timber, the screw would seek to deform within the soft layer and not break the harder modeled timber parts. After deforming, the displacement followed the surface. As the displacement followed the surface, and kept within the soft layer, the force was ultimately increasing and there were no sudden drop-offs in the force-displacement diagram, as was the case for the experimental tests. As seen in figure 4.4 there was a drop off later after the buckled shape appeared. This was solved by manually looking at the force/time graph to see if there were any disturbances in the graph. Seen with the small disturbance in figure 4.4 . Secondly, as buckling is a sudden change of shape, the deformed shape was looked at in Abaqus to see when the buckling shape took place. By finding the increment for when the buckling happened and reading the graph, the maximum load was found.

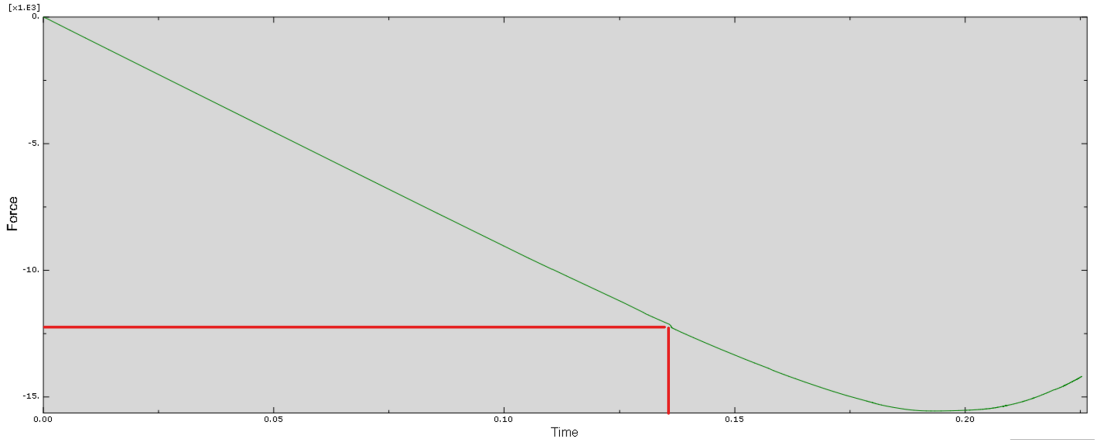

Figure 4.4: Test setup

4.2 Lab tests

4.3 Lab tests

Figure 4.5: Test setup

This test was carried out as a follow-up to the test carried out by Haande and Thunberg(3) in 2022 as part of their master thesis. Thus, the methods used are largely similar, but there are some differences. The scope of this investigation is also far greater as they only did this as a minor part of their research. The aim of this test is to measure the maximum capacity and look at the fracture mechanism. Where buckling and coaxing are the two possible outcomes.

4.3.1 Timber characteristics

The glue laminated timber used for these tests was GL 30 C from Moelven. The GL specimens used was previously used for reinforced pressure perpendicular to grain tests. The visible damaged timber was cut away, and the spare parts was used for this test. The two types of cross-section used was 140 x 225 mm and 140 x 540 mm with different lengths, respectively around 330 mm and 510/570 mm. The 140 x 225 mm was used for the 6mm test while 8 and 10mm tests were carried out on 140 x 540 mm. Meaning the screws inserted in the small samples would have one lamella (45 mm) less of high density timber, whilst the screws inserted in the large samples had two lamellas (90 mm) of high density timber. The specimens came from storage in an open garage, so the moisture content had been higher than 12 %. There was not enough time for the timber to condition in accordance to EN 408 within the time frame of this thesis. The specimens were only stored a few days in 20% humidity at 20°C. Figure 4.6 shows the moisture distribution on a specimen that is not properly conditioned. As the screws are in the middle layer the moisture in the middle the moisture had to be measured.

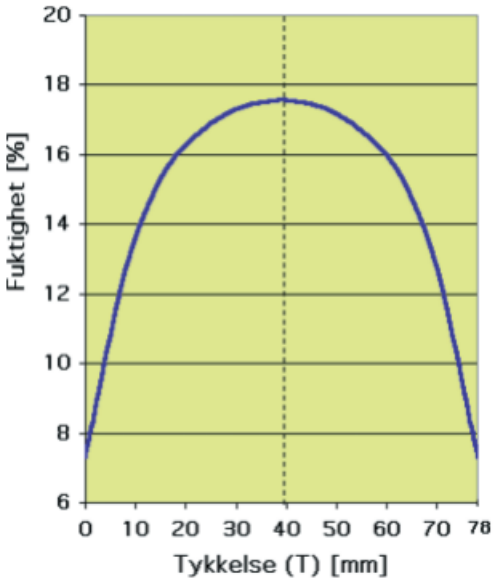

Figure 4.6: Moisture curve

In addition to describing conditioning EN 408 also states that moisture content should be taken a section from the test piece free from knots, and for perpendicular to grain tests specimens one should take these tests before the test an after conditioning. For this test with short conditioning time, the tests had to be done in the middle layer in order to get the correct moisture content around the screws. The moisture content was measured both on the outside and in the middle section close to the screw with Delmhorts RDM3 in accordance with EN 13183-2. This was done inserting the electrodes, seen in figure

4.7, around 2 cm into the timber. It should be noted that the values found was only measured in the same zones as the screws, meaning the timber beneath was neglected.

Figure 4.7: Delmhorts RDM3(9)

Due to being a key factor and using combined glue laminated timber, the density was measured in both the middle and upper layers. The density was measured after the test in a region not visibly damaged. EN 408 specifies that density should be controlled before compressing the timber. This was, however, not possible while keeping the end distances for the screws. The timber at the end should also have been quite unaffected by these tests. SKANORM 4, described in Kučera (31), was the basis of the method used for deciding the density. Following the demand of precision form ISO 13061-2 that states that a method with a precision the nearest 0,01 cm^3 or 3% is good enough . Mettler Toledo PG5002-s Delta range, seen in figure 4.8, was capable to measure within these demands.

Figure 4.8: Volume measuring using water imersion (10)

The density was measured using the following method:

1. The piece was weighed.
2. Before the water immersion, the test pieces were dipped into water and then dried with paper to prevent them from absorbing water during the volume measurement, and thus swell.
3. The volume of the piece was measured by water immersion. As seen in figure 4.8 dipping the piece into a bowl of water with a needle. The increased weight in gr is converted to mm^3.
4. The 12% density (ρ_{12}) was calculated using the moisture content (denoted as W), raw density (denoted as ρ_W), using the formula below stated in ISO 13061-2:

$$\rho_{12} = \rho_W \frac{1 + 0.01(12 - W)}{1 + 0.01(12 - W)\frac{\rho_W}{\rho_{H_2o}}} \tag{4.1}$$

The oven drying method, in accordance to EN 13183-1, was used later in order to approve the initial results. Were the section was dried in an aired oven at $103 \pm 2°C$. Were the same weighing and volume measuring as previously described followed to find the dry density. It should be noted that the weight of the glue is neglected, as it contributes to less than 1% of the total weight (18).

4.3.2 Screw characteristics

The screws used was HECO-TOPIX-plus with countersunk heads produced by HECO-Schrauben GmbH & Co and delivered by SFS Norway. With size ranging from 6 x 100 mm to 10 x 340 mm. Per screw type there are 3 types of transverse incline 0°, 5° and 10°. All three was repeated 3 times per screw, a total of 9 screws. The screws were screwed so deep that the screw-head was flush with the surface of the specimen, as seen in figure 4.9. The black lines illustrates the screws.

Figure 4.9: Inserted screws

The placement of the screws was so that the centre of gravity is in the middle of of the cross- section as seen in figures 4.9 and 4.10. Holes for the screws was pre-drilled in order to assure correct inclination, the pre-drilling holes was according to the ETA and was as long as the screw in accordance with EN 1995. The drilling was done with a drill from Meec tools for the 6mm screws and Dormer for the 8mm and 10mm. The straight holes were drilled with a bench drill press while the angled holes were made with a guide and drill.

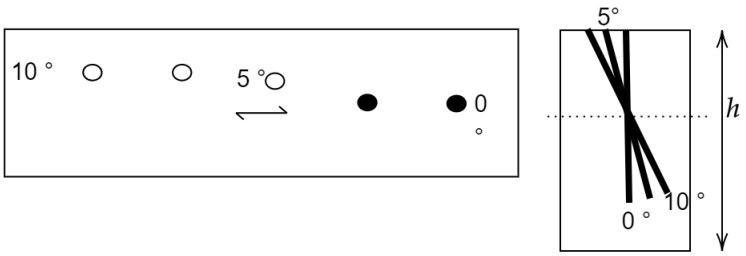

Figure 4.10: Placement of screws

The distances between the screws was decided by the amount of test material and proved to be greater than the values in EN 1995, and is displayed in table 4.3.

Diameter	C/c (mm)	Distance to end(mm)
6mm	80	80
8mm	80	80
10mm	100	120

Table 4.3: Screw distances

4.3.3 Test set up

The specimens was placed in a ZwickRoell Z1200 and pressed down on the screw with a bits fitting the trace of the screw head. This was done for about 30% of the tests, but it proved to be to time consuming to fit the torx with the time available on the lab. Therefor, it was decided to remove the traces on the torx in order to be able to do the tests at a higher tempo. The ZwickRoell Z1200 measured both total force and displacement on the screw. On the outside of the specimen, on both sides, aluminum brackets was screwed with small screws. Where the small screws was horizontally in line with the screw tip of the tested screw. This can be seen in figure 4.11, where the black line was drawn on the timber were the screws ended in order fit the screw in the correct place. Deformation sensors from Heidenhain (type BX-CNINCAD.YC1-001) was then placed below the brackets. This was done in order to measure the deformation in the screw length alone. By withdrawing the deformation below the screw measured by the sensors from Heidenhain, from the total displacement measured by the ZwickRoell the isolated displacement of the screw length was obtained.

Figure 4.11: Deformation sensors

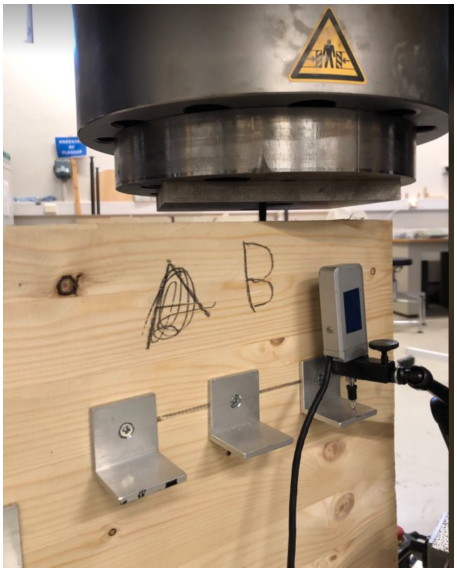

4.3.4 Test protocol

The tests were conducted in accordance with ISO 6891. The estimated load, F_{est}, was calculated using the proposal by Alosio et al.(7), following the formulas outlined in EN 1995 with slight modifications: α_g and the amplification factor, N_{ki}, were set at 0.16 and the latter was multiplied by 1.17 respectively. The push-through failure was calculated without any deviations from EN 1995. The screw head was neglected in the calculation.

The loading procedure, as described in ISO 6891, unfolded as follows. Firstly, F_{est} was calculated, taking into account both potential buckling failure and push-in failure (screw pressed in without buckling). The lowest strength failure mode was then selected. The application of load was carried out as illustrated in Figure 4.12, at a rate of $0.2F_{est}$ per minute until reaching $0.4F_{est}$, which was then held for 30 seconds. Subsequently, the load was reduced at the same speed to $0.1F_{est}$ and maintained for another 30 seconds. From there, the load was increased at the same speed up to $0.7F_{est}$. Beyond this point, in the red line, the loading rate was adjusted to maintain a constant rate of slip until either the ultimate load was reached or a slip of 15 mm occurred within 3 to 5 minutes (600-900 seconds), as shown in Figure 4.12.

The illustration in Figure 4.12 was based on a figure from Tomasi et al.(11). The constant rate of slip was the critical determinant during testing. This slip rate was informed by previous tests conducted by Haande and Thunberg(3) and was further optimized following initial tests which aimed to reach failure at around 4 minutes, the median value. All procedures adhered to ISO 6891:1991.

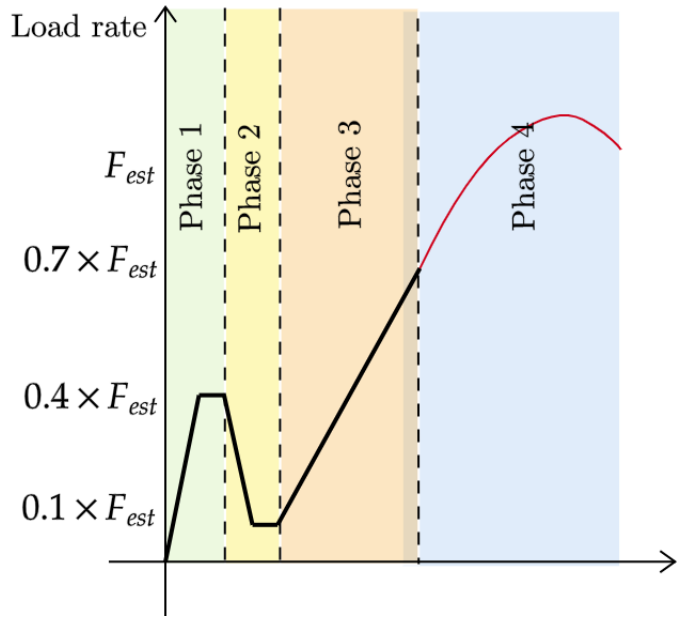

Figure 4.12: Load application ISO 6891:1991(11)

4.3.5 Extracting results

Due to this being a solution to cope with compression perpendicular to grain the F_{est} is estimated as described by EN 408. As previously described the F_{est} was calculated for the tests, this is from now on referred to as $F_{est,calc}$. En 408 describes a formula to get the elastic modulus. This formula was adapted to this test as seen below.

$$E = \frac{0.4F_{est} - 0.1F_{est}}{w_{40} - w_{10}} \tag{4.2}$$

The F_{est} estimation is an iterative procedure similar to the one described in EN 408 and by Tomasi et al.(11). Were the E-modulus is taken between 0.1 F_{est} and 0.4 F_{est}, as displayed in line 1 in figure 4.13. Line 1 was then moved 1% of the length of the screw, as displayed with line 2 in the same figure. The intersection between the second line and the force displacement graph was the estimated F_{est}, as displayed in figure 4.13. If the difference between the calculated F_{est} and the estimated F_{est} is greater than 5% this process is repeated until it is within the tolerance of 5%, replacing the calculated F_{est} with the estimated F_{est} This process was preformed using the script in appendix A.

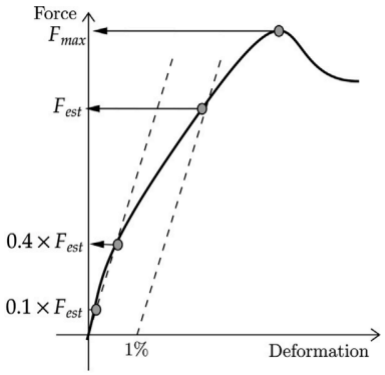

Figure 4.13: F_{est} basend on Tomasi et al.(11)

5. Results

In this chapter the results form both the experimental campaign with lab tests and numerical analysis in Abacus will be presented.

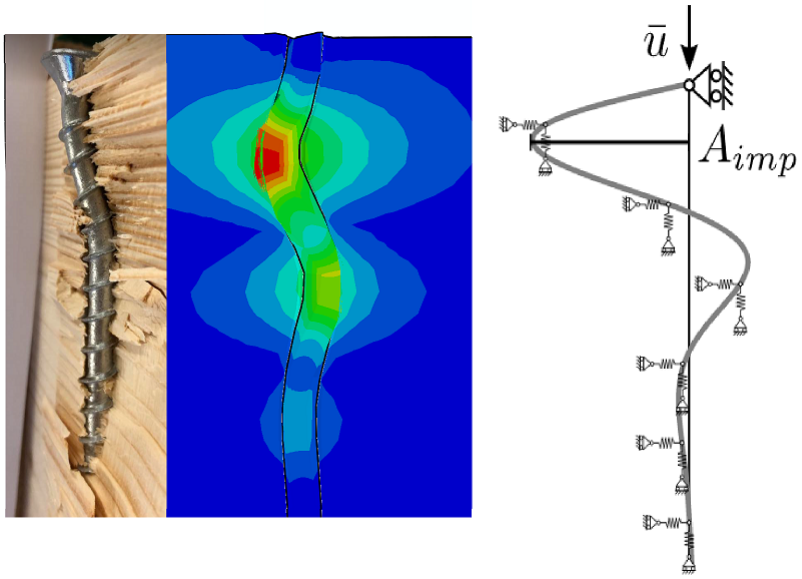

Figure 5.1: Results experimental, numerical and calculated

5.1 Experimental results form the lab

5.1.1 Failure modes

The failure modes was divided into two main failure categories, buckling and push trough. The buckling was, as seen in figure 5.2, at approximately the same distance from the screw head independent of the length of the screws. The buckling appeared on average at 2.5 cm $\pm$ 1 cm from the load application point. Buckling was there after divided into two sub categories. Buckling perpendicular and buckling longitudinal, meaning whether the buckling was orientated along or perpendicular to the grain direction.

Figure 5.2: Buckled screws

The push trough failure, as seen in figure 5.3 is a combination of failure in the radial-lateral and radial-tangential planes. According to Ringhofer(4) the mechanical properties in these planes is different. Where the shear moduli ratios between the two planes ranges between 13:1 and 30:1 causing an inhomogeneous failure around the screw. The dispersion and the size of the stressed timber volume depends on the fibre orientation and can not be described by a cylindrical surface. Figure 5.3 displays a cut along the grain, displaying the tangential failure.

Figure 5.3: Push trough failure

In addition to the two mentioned failures, it must be mentioned that there is a combined failure as well. Some of the screws had a buckling shape, but also signs of push trough failure. If the push in caused the buckling due to redistributing the load unsymmetrical, or the buckling happened at the same time as push trough because it had reaced the buckling load is hard to tell with so few tests. The test set up was not focused on this, and thus the amount of data on this is scarce. The screws is noted as combined in the tables, but included as buckled in the graphs and statistics as they have in fact buckled.

5.1.2 Tabulated results

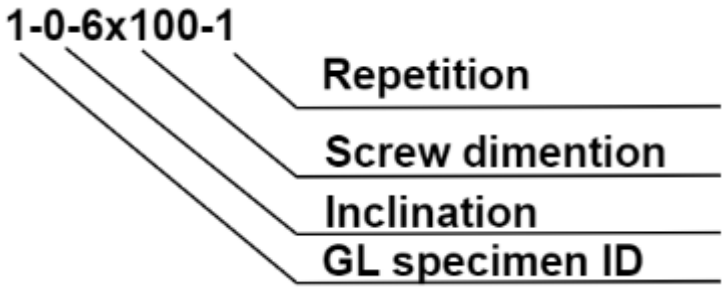

Figure 5.4: Explanation of the name tag

Figure 5.4 displays what the different values in the name tag indicates. GL specimen ID is simply the number assigned to the glue lam piece the screw in question was inserted into. As previously stated the inclination varies from 0 to 10 degrees, as is displayed in the second parameter. Screw dimension is just that. Repetition refers to the test number for a inclination for a single screw type. It is important to note that the GL-specimen does not affect the repetition parameter, just inclination and screw type.

Table of timber measured characteristics

These were the results form the described testing done on the timber specimens. The results presented is the first measured with humidity. The oven drying method verified that the method adjusting the density from the measured humidity was good enough for this purpose. All tests within +- 6% of the initial result, and on average 4% lower than the initial result. This was deemed good enough for further use.

Table 5.1: Results timber tests

	Density ρ_{12} (kg/m^3)		**Humidity** (%)	
Gluelam Specimen ID	**Upper**	**Middle**	**Upper**	**Middle**
1	483	480	15	16
2	520	540	17	18
3	465	437	17	16
4	518	453	17	17
5	513	435	18	15
6	489	459	16	16
7	455	514	16	17
8	446	444	16	18
9	475	491	15	17
10	521	524	17	16
11	496	453	7	13
12	447	446	16	16
13	420	430	16	15
14	426	420	16	16
15	466	440	16	16
16	427	437	15	14
17	461	445	16	15
18	405	486	17	19
19	451	432	16	16
20	440	433	16	18
21	421	460	14	16
22	532	450	15	20
23	506	524	14	18
24	500	534	17	14
25	507	482	15	10
26	483	476	18	12

Results table 6mm screws

All of the 6mm screws had the same failure mode, push in. F_{est}* is the calculated value before the test and F_{est}** is the value estimated in accordance to the description in the methods chapter. This also applies to all the similar tables below. F_{est}** was in general estimated on the first attempt, some required two estimations.

Table 5.2: Results 6mm screws

Test code	**F$_{est}$*** $[N]$	**Failure mode Calculated**	**F$_{max}$** $[N]$	**Failiure mode Experimental**	**Buckling direction**	**F$_{est}$**** $[N]$
1-0-6x100-1	10805	P	9368	Push trough		7926
1-0-6x100-2	10805	P	9647	Push trough		7933
1-0-6x100-3	10805	P	12451	Push trough		9041
2-5-6x100-1	10627	P	9509	Push trough		8060
2-5-6x100-2	10627	P	10350	Push trough		8098
2-5-6x100-3	10627	P	9168	Push trough		7891
3-10-6x100-1	10934	P	12116	Push trough		9033
3-10-6x100-2	10934	P	10599	Push trough		8231
3-10-6x100-3	10934	P	11159	Push trough		8126
4-0-6x120-1	13092	P	11129	Push trough		9027
4-0-6x120-2	13092	P	12352	Push trough		9352
4-0-6x120-3	13092	P	11838	Push trough		9603
5-5-6x120-1	13293	P	10770	Push trough		8971
5-5-6x120-2	13293	P	10685	Push trough		9080
5-5-6x120-3	13293	P	10356	Push trough		9313
6-10-6x120-1	13061	P	11535	Push trough		9552
6-10-6x120-2	13061	P	10656	Push trough		9317
6-10-6x120-3	13061	P	12275	Push trough		10148
7-0-6x160-1	15085	B	13891	Push trough		16369
7-0-6x160-2	15085	B	12294	Push trough		14619
7-0-6x160-3	15085	B	13272	Push trough		16178
8-5-6x160-1	15157	B	12336	Push trough		14075
8-5-6x160-2	15157	B	12717	Push trough		14225
8-5-6x160-3	15157	B	12067	Push trough		14368
9-10-6x160-1	15126	B	12843	Push trough		16954
9-10-6x160-2	15126	B	11335	Push trough		13656
9-10-6x160-3	15126	B	11654	Push trough		11654

Results table 8mm screws The 8mm screws had all three failure modes. For further investigations combined failure is noted as buckling as the screws buckled. F_{est}** was in general estimated on the first or second attempt. In some cases the 1% rule when estimating was not able to obtain and F_{est} was set equal to F_{max}. This was due to sudden decrease in load bearing capacity, causing the test to end in accordance to ISO 6891 as previously described.

Table 5.3: Results 8mm screws (P=perpendicular L=longitudinal)

Test code	**F**$_{est}$* $[N]$	**Failure mode Calculated**	**F**$_{max}$ $[N]$	**Failiure mode Experimental**	**Buckling direction**	**F**$_{est}$** $[N]$
10-0-8x120-1	17644	P	18032	Push trough		14574
10-0-8x120-2	17644	P	18129	Push trough		14670
10-0-8x120-3	17644	P	19052	Push trough		15063
11-5-8x120-1	15177	P	18327	Push trough		14611
11-5-8x120-2	15177	P	17335	Push trough		13710
11-5-8x120-3	15177	P	18053	Push trough		14354
11-10-8x120-1	15177	P	16596	Push trough		13428
11-10-8x120-2	15177	P	15777	Push trough		12708
12-10-8x120-3	15177	P	21814	Buckle	P	15926
10-0-8x160-1	23546	P	27498	Push trough		24147
10-0-8x160-2	23546	P	25446	Combined	P	21539
13-0-8x160-3	23546	P	24701	Buckle	P	20910
12-5-8x160-1	23522	P	25353	Push trough	P	21712
12-5-8x160-2	23522	P	25892	Push trough	L	23253
12-5-8x160-3	23522	P	23820	Buckle	P	20419
14-10-8x160-1	22890	P	22696	Combined	L	19221
14-10-8x160-2	22890	P	26039	Push trough	L	23545
14-10-8x160-3	22890	P	23945	Push trough	L	19516
13-0-8x200-1	27271	B	29671	Combined	P	29662
13-0-8x200-2	27271	B	30898	Combined	P	30669
13-0-8x200-3	27271	B	25629	Buckle	P	25461
14-5-8x200-1	27141	B	26046	Buckle	P	23564
14-5-8x200-2	27141	B	26036	Buckle	L	19425
15-5-8x200-3	27136	B	24243	Buckle	P	25660

Test code	**F**$_{est}$* $[N]$	**Failure mode Calculated**	**F**$_{max}$ $[N]$	**Failiure mode Experimental**	**Buckling direction**	**F**$_{est}$** $[N]$
15-10-8x200-1	27136	B	23575	Buckle	P	25806
15-10-8x200-2	27136	B	19538	Buckle	P	24056
15-10-8x200-3	27136	B	20513	Buckle	P	20364
16-0-8x220-1	27146	B	21992	Buckle	P	21974
16-0-8x220-2	27146	B	29007	Buckle	P	28871
16-0-8x220-3	27146	B	31018	Buckle	P	30988
16-5-8x220-1	27146	B	30014	Buckle	P	29726
16-5-8x220-2	27146	B	29229	Buckle	L	29175
17-5-8x220-3	27049	B	24367	Buckle	P	23852
17-10-8x220-1	27049	B	21736	Buckle	P	21493
17-10-8x220-2	27049	B	24695	Buckle	P	24663
17-10-8x220-3	27049	B	23475	Buckle	P	23449
18-0-8x260-1	27164	B	26907	Buckle	P	26907
18-0-8x260-2	27164	B	28453	Buckle	P	28399
18-0-8x260-3	27164	B	29055	Buckle	P	28499
18-5-8x260-1	27164	B	22319	Buckle	L	22208
19-5-8x260-2	27257	B	18744	Buckle	L	18744
19-5-8x260-3	27257	B	27232	Buckle	P	26583
19-10-8x260-1	27257	B	25875	Buckle	P	25086
19-10-8x260-2	27257	B	26184	Buckle	P	25685
19-10-8x260-3	27257	B	26392	Buckle	P	26171
20-0-8x280-1	27115	B	18805	Buckle	P	18805
20-0-8x280-2	27115	B	26184	Buckle	P	26184
20-0-8x280-3	27115	B	27090	Buckle	P	27090
20-5-8x280-1	27115	B	25174	Buckle	L	24414
20-5-8x280-2	27115	B	26386	Buckle	L	26386
21-5-8x280-3	27054	B	25382	Buckle	P	25382
21-10-8x280-1	27054	B	22084	Buckle	P	22084
21-10-8x280-2	27054	B	24269	Buckle	P	24269
21-10-8x280-3	27054	B	22145	Buckle	L	21488

Results table 10mm screws

All the 10mm screws buckled. For this dimension F_{est}** was in general estimated on the first or second attempt, or not possible to estimate. If it was not possible to estimate it was put as the same value as F_{max}, like it was done for the 8mm screw. For these tests it must be mentioned that there were some trouble preforming the tests as the torx broke on several of the tests and had to be restarted.

Table 5.4: Results 10mm screws (P=perpendicular L=longitudinal)

Test code	**F**$_{est}$* $[N]$	**Failure mode Calculated**	**F**$_{max}$ $[N]$	**Failiure mode Experimental**	**Buckling direction**	**F**$_{est}$** $[N]$
22-0-10x300-1	42481	B	37598	Buckle	P	37598
22-0-10x300-2	42481	B	38586	Buckle	P	39054
22-0-10x300-3	42481	B	43432	Buckle	P	43491
23-5-10x300-1	42649	B	31223	Buckle	L	32279
23-5-10x300-2	42649	B	34996	Buckle	L	35637
23-5-10x300-3	42649	B	35797	Buckle	L	35116
23-5-10x300-1	42649	B	31383	Buckle	L	31410
24-10-10x300-2	42616	B	31579	Buckle	L	31690
24-10-10x300-3	42616	B	29832	Buckle	L	30481
25-0-10x340-1	42586	B	35737	Buckle	L	35737
25-0-10x340-2	42586	B	39221	Buckle	P	39221
25-0-10x340-3	42586	B	39222	Buckle	P	39222
25-5-10x340-1	42586	B	38091	Buckle	P	38091
26-5-10x340-2	42751	B	35523	Buckle	P	36377
26-5-10x340-3	42751	B	39413	Buckle	P	39413
26-10-10x340-1	42751	B	38398	Buckle	P	38398
26-10-10x340-2	42751	B	38225	Buckle	P	38225
22-10-10x340-3	42481	B	35513	Buckle	L	35800

5.2 Numerical results

5.2.1 Final numerical study

The results from the numerical buckling analysis is divided into inclination, as seen in table 5.5, and density, as seen in table 5.6. The 0°tests was conducted using buckling step in Abaqus, while the inclined screws was conducted using imposed displacement.

Inclination	8mm	10mm
0°	32.4 kN	38 kN
5°	26 kN	30 kN
10°	19.7 kN	23.9 kN

Table 5.5: Numerical results inclination

Density	8mm	10mm
High density (450 kg/m^3)	35.1 kN	38 kN
Medium density (490 kg/m^3)	32.4 kN	35.1 KN
Low density (520 kg/m^3)	28.6 kN	30.2 kN

Table 5.6: Numerical results density differentiated tests.

5.2.2 Initial numerical study

The results seen in table 5.7 is from replicating studies done by Haande and Thunberg(3).

Test	Numerical results
S_8.0_200_B	219 kN
Pe_7.0_160_B	167 kN
Pe_8.2_160_B	169 kN
Pe_8.0_200_B	177 kN

Table 5.7: Numerical results initial study

6. Discussion

6.1 Validation of numerical campaign

Figure 6.1: Comparison results

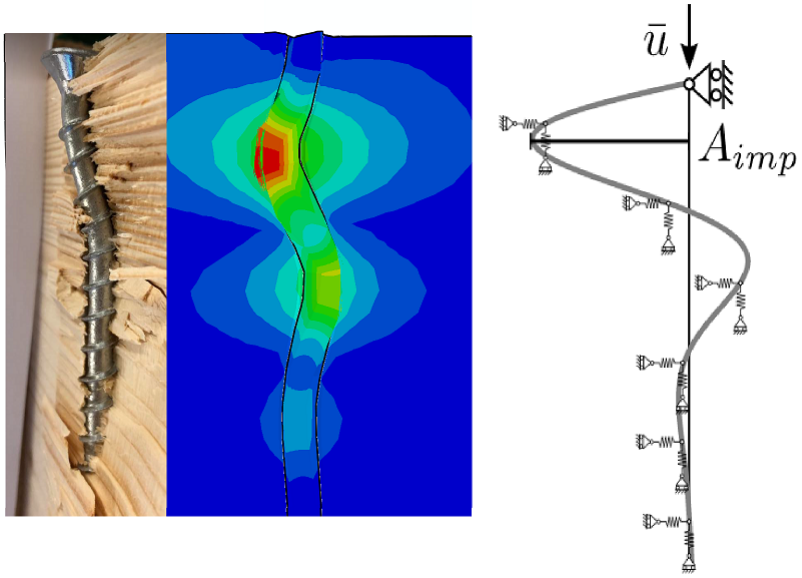

The numerical results, both for the 0-degree inclination using the buckling step and the inclined calculations using non-linear methods with imposed displacement, showed similar buckling modes and loads to the experimental tests. These results were also consistent with the failure described by Alosio et al.(7). Furthermore, the load results were quite similar to those obtained from testing and calculations. The majority of the input was based on factual values, suggesting that the model appears to be accurate.

One potential limitation of the numerical study is the use of the buckling step for the 0-degree tests. The buckling step is a linear method. As explained previously, it solves an eigenvalue problem, predicting the strength in an idealized, elastic manner. This may not fully capture the complexities of real-world conditions and behaviors, as previously stated. Non-linear methods, can provide a more accurate prediction of the buckling load and post-buckling behavior.

Despite this limitation, the numerical study provided valuable insights into the buckling behavior of the screws and validated the experimental results. However, further studies using non-linear methods for all inclinations and considering potential imperfections in the screws and timber could further enhance the accuracy of the model.

6.2 Numerical results

The results from Abaqus primarily focus on the buckling load. As both the soft layer and interaction property have been modeled based on experimental results and, as previously described, were determined through an iterative process. Thus, the results are somewhat fabricated as a product of this iterative process, and the force/displacement was not considered to be as interesting as the buckling loads.

The buckling load, however, is not based on such an iterative process. The interaction between the screw and timber perpendicular to the screw in both longitudinal and transverse directions of the timber has been tested by Bjetka and Blass (6). Thus, the buckling support from the timber should be accurate.

6.3 Experimental data

All the graphics in this chapter are created using JMP statistical software. The displayed box plots are standard, showing the median as a line within the box. From the upper line and up in the box represents the fourth quartile, and the lower line represents the first quartile, meaning 50% of the data lies between these lines. The whiskers display the minimum and maximum values.

There are some values that are significantly high and low for each screw length and diameter. In some of the plots, these are noted as outliers and presented as dots. In others, they are included. This is dependent on the intention of the plot and the number of screws included in the plot. Several lengths share the same value, which means that when considering a larger data set, these results are not unique and therefore not considered outliers. In others, the filtering may cause these to appear as outliers compared to the other tests they are compared to.

When it comes to test time, the majority of test was within the specified time. However, some of the tests failed to reach failure within the specified time. The shorter screws on average had longer test time, and some even over the limit. A theory for the reasoning behind this was that the screw head increased the capacity, in a manner that the calculations did not account for, and that this had a higher contribution percentage wise than for the longer screws. There also seems to be correlation between screw angle and shorter test time even without buckling failure.

The longer screws, L>260mm, proved to be a stiff connection. This caused the calculation of F_{est} to be equal to F_{maks}.

6.3.1 Box plot of all dimensions by screw length

In Figure 6.2, a box plot presents the results of tests performed on the 6mm screws, categorized by their dimensions. Despite the 6x160mm screws being calculated to buckle, all of them failed due to push-through. The actual failure load in tests was approximately 30% less than the predicted buckling load. The 6x120mm screws were also within 20% of the calculated buckling load. Screws with larger diameters failed within this load range on several occasions, so it would not be unreasonable to expect buckling from these screws as well. However, the 6x120mm screws never reached the calculated failure load, and were consistently about 35% below the predicted failure load.

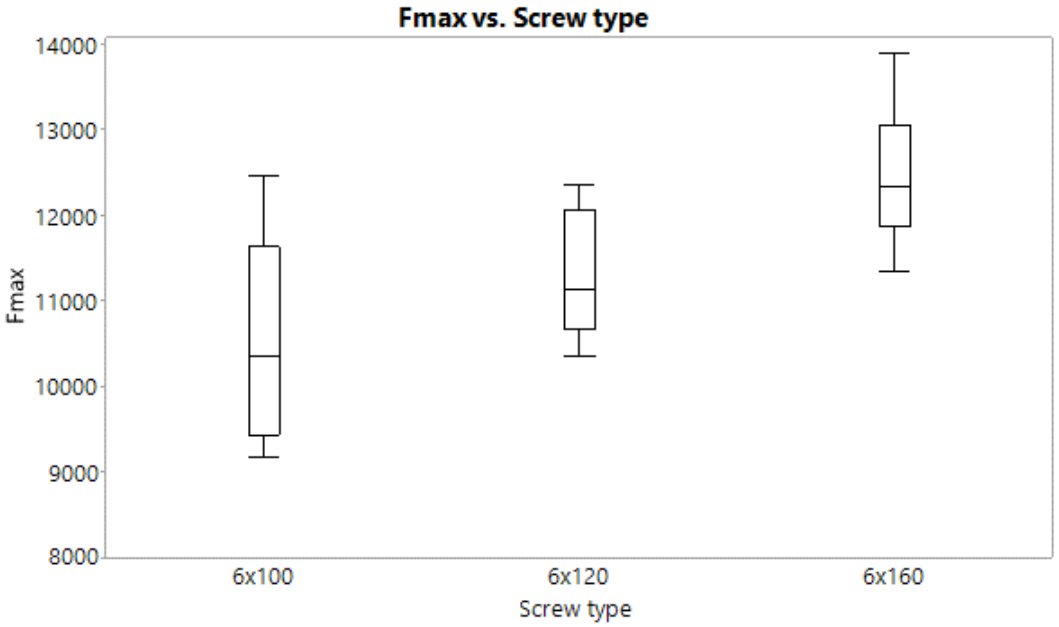

Figure 6.2: 6mm screws [Unit = N]

In the case of 6mm screws, despite the 6x160mm screws being calculated to buckle, all of them failed due to push-through. The actual failure load in tests was approximately 30% less than the predicted buckling load. The 6x120mm screws were also within 20% of the calculated buckling load.

Screws with larger diameters failed within this load range on multiple occasions, so it wouldn't be unreasonable to expect buckling from these screws as well. However, the 6x120mm screws never reached the calculated failure load, consistently falling about 30% below the predicted failure load.

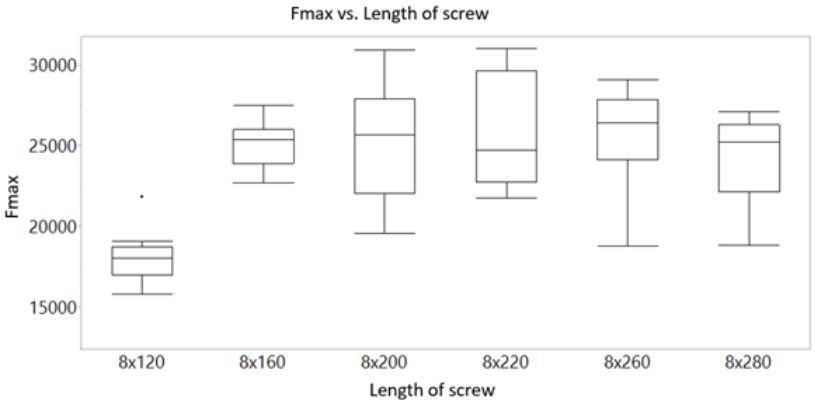

Figure 6.3: 8mm screws [Unit = N]

Like the 6mm and 8mm screws, the 10mm screws are presented in a box plot in Figure 6.4. The median for the two boxes is at about 35 kN and 38 kN. The expected value for this was in the region of 42 kN. Apart from one test, all of the screws were below 40 kN.

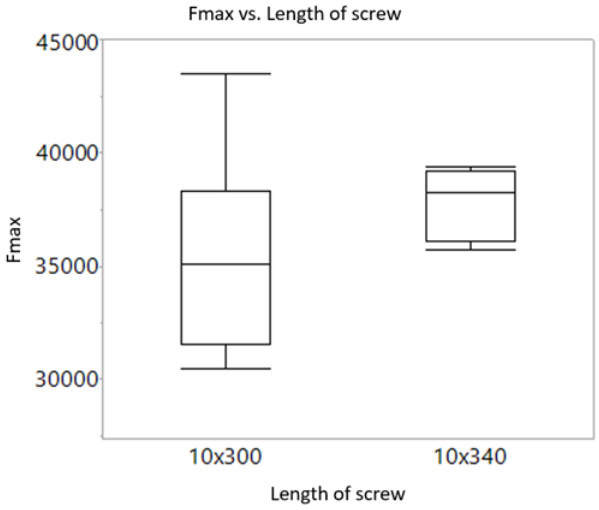

Figure 6.4: 10mm screws [Unit = N]

6.4 Inclination

The effect of inclination on capacity is evident in the box plot. The average capacity for screws at 0° being about $27kN$, at 5° being $25.4kN$, and at 10° being $23.4kN$, reinforces these findings. Some of the difference in buckling load for screws of varying lengths presented in the box plot may well be related to their density ass seen in the scatter plot.

Figure 6.5: Buckled screws [Unit = N]

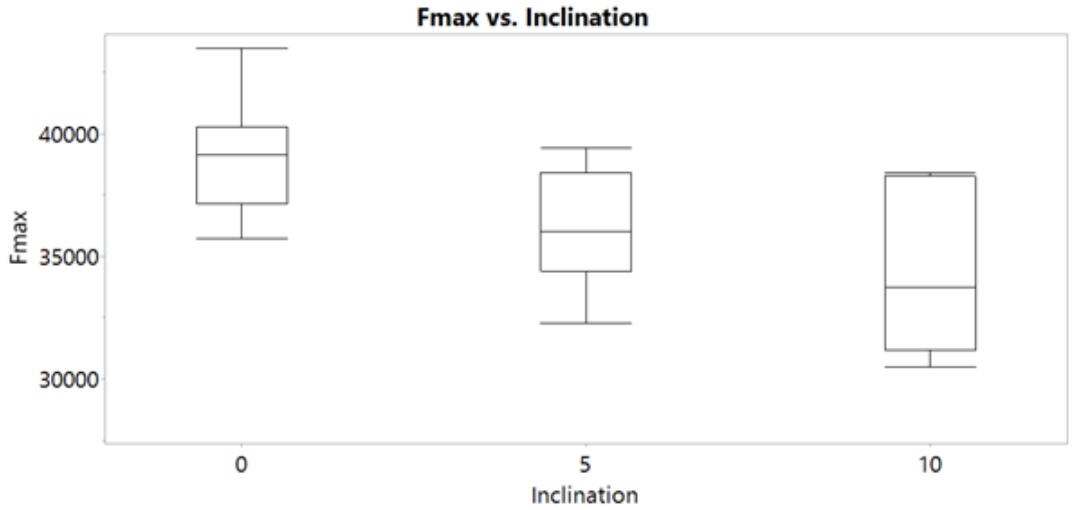

Figure 6.6: Buckled screws [Unit = N]

Figure 6.7 presents the buckling plots of 8mm and 10mm screws, with the former on the right and the latter on the left. The top row illustrates a 5° inclination, while the

bottom row represents a 10° inclination. Notably, the observed buckling modes matched our experimental results.

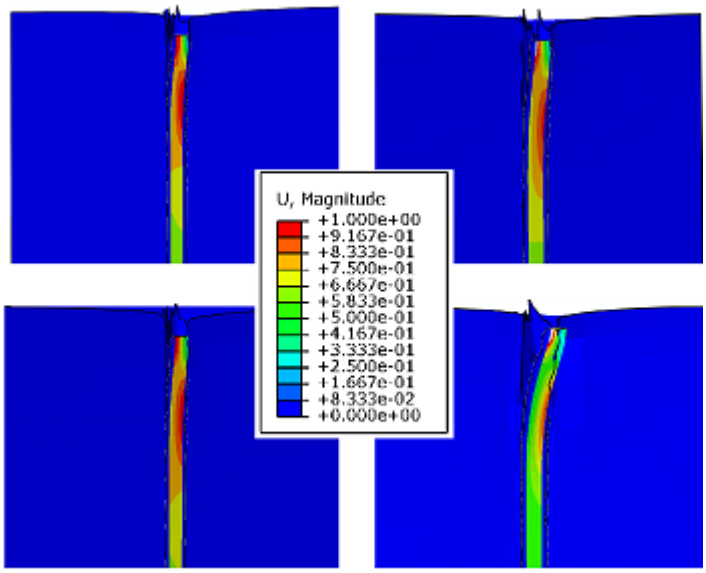

Figure 6.7: All inclined numerical tests. [Unit = N]
8mm is left, and 10mm is right. 5° top row and 10° bottom row

As displayed in table 6.1he calculated buckling load for the 8mm screws registered at 27.2 kN. For the 0° inclined 8mm screw, the output aligned with the experimental findings, which is encouraging given that it was anticipated a higher buckling load from numerical analysis. Inclination was found to significantly influence the reduction in buckling load across all cases. Considering this impact and the behavior of the 8mm screws, it appears reasonable to propose a higher reduction factor, α_g (initially suggested as 0.16). Adjusting this factor for 5° and 10° inclinations, sugest using $\alpha_{g,5} = 0.3$ and $\alpha_{g,10} = 0.5$. However, due to the limited number of tests and other uncertainties, like manufacturing of the screws, a precision of one decimal place was set.

Inclination	Numerical [kN]	Experimental [kN]
0°	32.4	27.4
5°	26	25.4
10°	19.7	23.4

Table 6.1: Buckling loads effect of inclination

For the 10mm screws, the calculated buckling load was 42.6 kN, exceeding the experimental result by 7% and the numerical result by 9.5%. Interestingly, the discrepancy between the numerical and experimental results increased with an increase in inclination. This inconsistency among results complicates the evaluation of α_g. As a result,

determining a suitable α_g for these tests becomes less relevant. However, using the previously suggested α_g, the decrease in kN aligned with the experimental tests, confirming that the effect of α_g is in the suggested region for each inclination.

Inclination	Numerical [kN]	Experimental [kN]
0°	38	39
5°	28.1	36.2
10°	23.9	34.3

Table 6.2: Buckling loads effect of inclination

6.5 Density

The line in this scatter plot is a cubic spline with lambda of 0.05 and standardized X values. Were the latter is the same as subtracting the mean and dividing by the standard deviation for the variable, in this case F_max.

The plot displays the increased capacity with increased density for the 8mm screws. High-density (510 kg/m^3 and upwards) tests generally exhibited a higher capacity (29.4 kN on average) compared to low-density (460 kg/m^3 and less) screws (23.8 kN on average) and medium-density (from 460 to 510 kg/m^3) screws (26.8 kN on average).

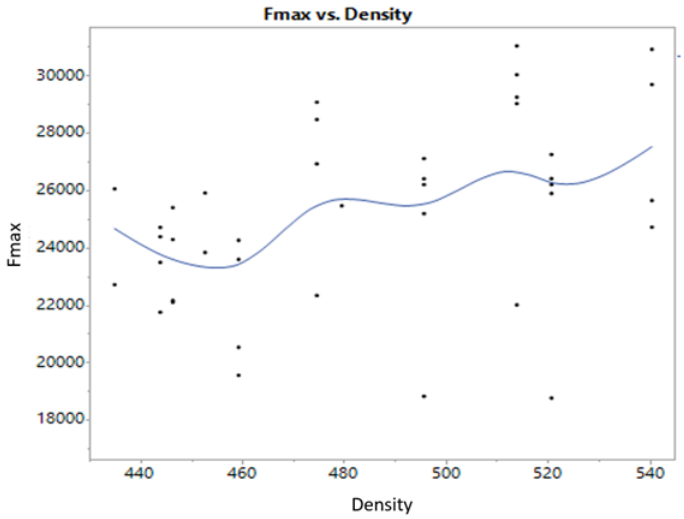

Figure 6.8: Buckled screws [Unit = N]

The plot for the 10mm screws does not directly provide the same conclusion. As there were fewer tests and a spread in density from 480 kg/m^3 to 540 kg/m^3. The tests did not provide enough data to achieve a similarly strong argument for increase in capacity. However, it still displays an increase in capacity. For the high, medium, and low-density tests, the average capacities were 38.1 kN, 38.0 kN, and 35.2 kN, respectively. This

indicates that the medium and high-density capacities were about 8% higher than the low-density capacity.

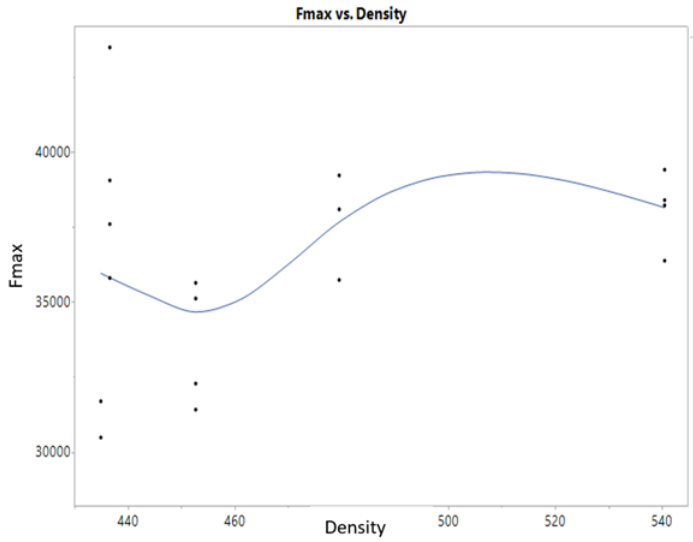

Figure 6.9: Buckled screws [Unit = N]

As previously mentioned the 0° inclined screws were only simulated using a linear approach providing a greater buckling strength. The bucklingmode was similar to the one found in the experimental tests, as displayed form low to high density in 6.9. The 8mm screws had more or less the same plots and is thus included.However, the aim for these test were to provide data confirming the findings in the experimental tests. As the increase in buckling strength was evident with greater density, the numerical tests confirms these findings.

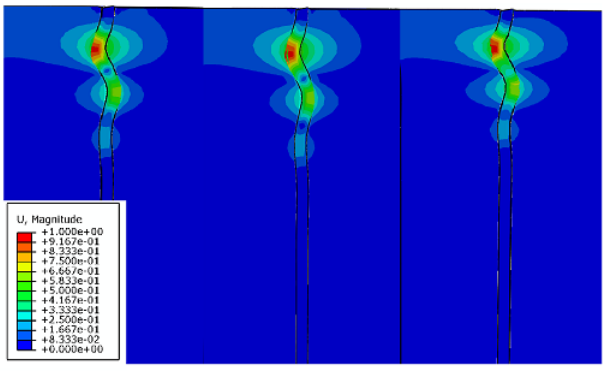

Figure 6.10: Results experimental, numerical and calculated

The 8mm screws also showed an increase in strength, as seen in Table 6.3, from low to medium density of 2.4 kN for the experimental tests and 3.8 kN for the numerical tests, respectively 10% and 13%. From medium to high density, the increase was 3.4 kN (12%) experimentally and 2.7 kN (11%) numerically. Again, the increase with higher density

is evident for both the numerical and experimental tests. However, the difference in strength for the calculation was just 0.3 kN from low to high density.

Density	Numerical [kN]	Experimental [kN]	Calculated [kN]
High density **>520** kg/m^3	27.4	29.4	27.4
Medium density **450-520** kg/m^3	25.9	26.8	27.2
Low density **<460** kg/m^3	23.5	23.8	27.1

Table 6.3: Buckling loads effect of density

The 10mm screws demonstrated an increase in strength, as shown in Table 6.4, from low to medium density of 5.7 kN for the experimental tests and 5.1 kN for the numerical tests. From medium to high density, the increase was 0.1 kN experimentally and 2.9 kN numerically. The increase with higher density is noticeable for both the numerical and experimental tests for this dimension. However, the difference in calculation was just 0.4 kN from low to high density.

Density	Numerical [kN]	Experimental [kN]	Calculated [kN]
High density **>520** kg/m^3	38	38.1	42.7
Medium density **450-520** kg/m^3	35.1	38	42.6
Low density **<460** kg/m^3	30.2	32.3	42.3

Table 6.4: Buckling loads effect of density

Figure 6.11 displays the C_h parameter for densities between 300 and 700 kg/m^3. As demonstrated, the difference between the categories in this thesis was between 130/160 and 140/170, with a minor difference between the diameters as well.

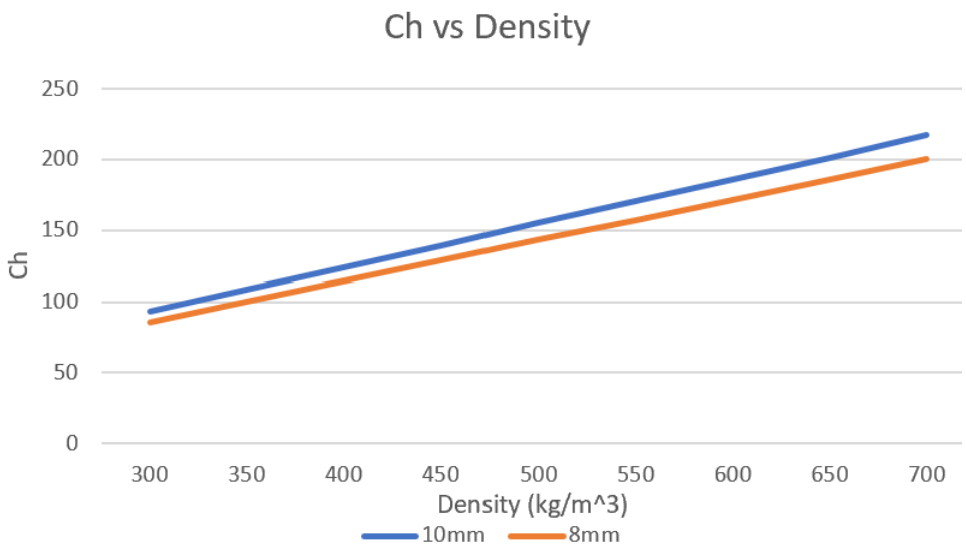

Figure 6.11: Correlation between density and C_h

Figures 6.12 and 6.13 illustrate the impact of density on the calculated loads, in orange, while the blue line represents the experimental increase, and the gray line indicates the numerical increase. There is a noticeable increase in strength for both numerical and experimental results, suggesting that the effect of C_h is underestimated in the current calculations. However, the spread in density is relatively small, and the increase is quite steep. The strength increase would not linearly continue up to 700 kg/m^3 as the area of the screw shank would not be able to sustain the load as the load would exceed flow stress limit.

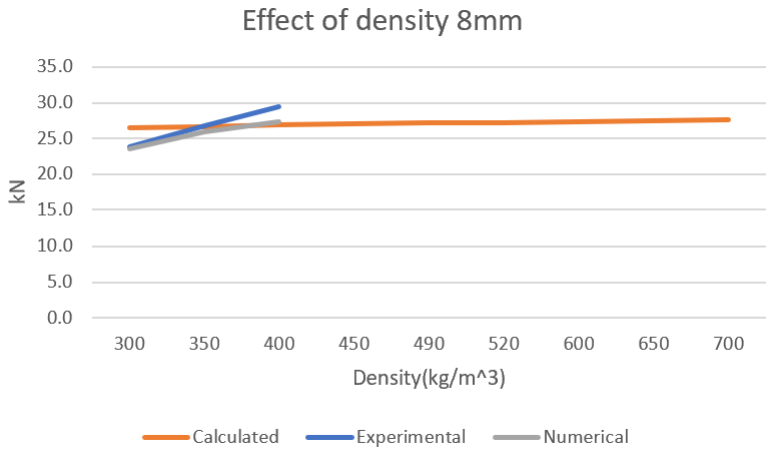

Figure 6.12: Correlation density buckling strength 8mm

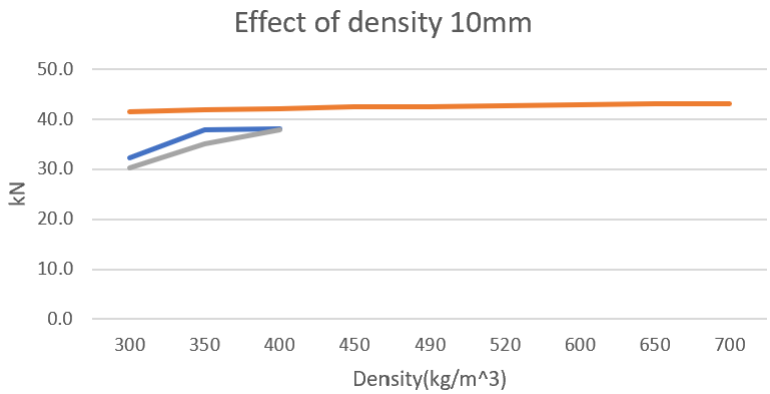

Figure 6.13: Correlation density buckling strength 10mm

6.6 Screws with combined failure

Combined failure occurred when the screws experienced both push-through and buckling failure. This failure mode may be among the most crucial to investigate closely due to the fact that, in cases of combined failure, the screw is fully utilized. This implies that from a materials perspective, it is the most efficient option for maximizing the screw's potential. However, in the experimental tests, only seven screws failed in this manner, providing limited data for analysis.

Due to natural differences in timber, it is hypothesized that the buckling of screws at the limit for both timber failure and screw failure may be influenced by localized failures in the timber. This could result in an uneven distribution of load on the gross section of the screw, meaning that some parts of the screw are subjected to greater stress than others, leading to buckling. It was challenging to find clear evidence supporting this hypothesis when inspecting the timber and screws, other than the fact that the buckling was not as pronounced on some of these samples. The observation that the buckling deformation on the screws is smaller for the longer screws, despite sharing the same deformation parameter from the test, could also support this hypothesis. This might suggest the occurrence of combined failure.

The examination of inclination revealed that minor inclinations did not impact screw capacity by more than approximately 8%. Since combined failure could only result in minor deflection (otherwise it would be categorized as a timber failure), this percentage is likely lower, suggesting that this failure mode is not a major source of uncertainty.

6.7 Sources of error

6.7.1 Screws

All the screws were carefully inspected for any visible defects or issues before and after failure. When inspecting the screws it was observed a lot of minor imperfections. Some screws had minor indent's, and many of them had visible differences in the traces. These errors occurred on the same location of the screws suggesting that the error stems from the cold forming process. Specifically the 8x220 and 260 screws had visible defects in the tracings at the same location. It was not possible to document this with a normal camera, due to the defect being so small. The 8x220 screw had this imperfection closest to the screw head at about 5-6 cm for a few rounds of tracing around the screw. For these tests it was not noticeable in the results that this was the reasoning for systematic failure. However, this indicates that the production process for the screws not is perfect and, that other defects may have been present but not located. This might be a cause for outliers as well as the timber. Outliers were more thoroughly examined, but it was hard to identify any reasons for failure in the screws.

Both density and inclination appeared to have an effect on the average capacity. However, the similar spread of results for both straight and inclined screws, as well as low and high-density tests, suggests that other factors may have a more significant influence on capacity than these parameters. Another indication of this is the varying buckling direction for different inclinations. If timber were the major deciding factor, screws would predominantly buckle perpendicularly. The buckling directions were as follows:

- Longitudinal buckling: 37.5% of all screws
- Longitudinal buckling: 48% of the 5% inclined screws
- Longitudinal buckling: 28% of the 10% inclined screws

The fact that even inclined screws buckled longitudinally, more so than straight screws, points to the existence of other significant determining factors. Theoretically, inclined screws should have eccentricity and thus buckle in the inclined direction. The cause for the higher prevalence of longitudinal buckling in inclined screws is currently unknown. As shown in the table for 8mm and 10mm screws, longitudinal buckling seemed to occur in clusters, but the reason for this is still speculative. Possible explanations could include variations in thread, defects in the screws appearing at the same location, or unidentified defects/impurities in the timber. The limited number of tests to base this on, with only about 20 tests for each inclination with buckling, also poses a challenge. Load application may also have influenced the results, as fitting the torx into the screw was difficult, potentially inducing unintended eccentricities.

6.7.2 Timber

As previously noted, the timber specimens had been utilized in a thesis last year, researching compression perpendicular to the grain. Visibly damaged timber was discarded, and the remaining pieces were used for this study. Additionally, the specimens had been stored outdoors under a roof or in an open garage, resulting in high moisture content that was not fully dried out prior to testing due to time constraints, as mentioned earlier. As depicted in Figure 6.14, significant cracks were evident in the timber. These were avoided as much as possible and were only present in the 10x300 screws and one 10x340 screw (the last screw). To the best of my knowledge, after inspecting the results, these defects did not appear to affect the outcomes. The test setup also mitigated this issue, as the Heidenhein measurement method focused solely on the screw.

Figure 6.14: Defects in timber

As stated, the glue was not accounted for in this study. Since the glued layer was situated 45 mm from the top of the specimen and the screw head was embedded into the timber, the distance between the glued layer and the buckling failure point was less than than 20 mm. This could potentially influence the results.

6.7.3 Screw head

There are some differences in the buckling loads between the experimental and numerical results. Some of these differences might be attributed to the fact that the screw head is not included in the model. This was a deliberate decision for several reasons:

- First, the objective was to understand the buckling load across all manufacturers.
- Second, different manufacturers produce screws with diverse head designs. As such, the numerical study would only be directly applicable to the specific screws under consideration, limiting its broader applicability.

- Finally, the modeling technique and method derived from the initial studies may not be suitable for capturing the indentation caused by the screw head, due to the use of the soft layer.

Given these considerations, it is crucial to recognize the limitations introduced by not incorporating the screw head into the model, and to discuss how this might have impacted the buckling load results. By calculating the head pull-through resistance according to EN 1995, it could be inferred that the screw head may influence the results by around 1-2 kN, as indicated by Equation 6.1.

$$F_{ax,\alpha,R_k} = f_{\text{head},k} \cdot d_h^2 \cdot \left(\frac{\rho_k}{380}\right)^{0.8} \tag{6.1}$$

6.8 Evaluation of initial numerical campaign

This study has yielded some intriguing findings. Firstly, as illustrated in Figure 6.15, the buckling modes closely resemble those observed during the torx tests. This suggests that the tests performed offer a reasonably accurate simulation of the screw behavior when used with a steel plate.

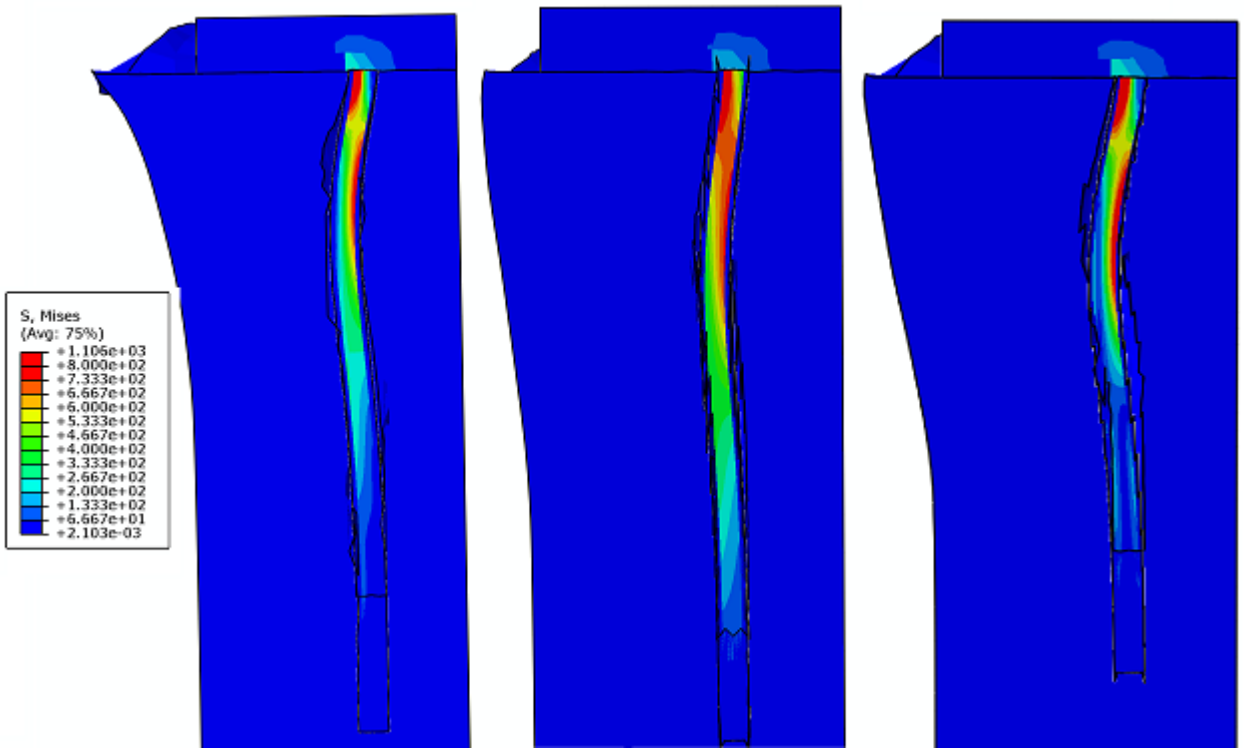

Figure 6.15: Plots of initial simulations in Abaqus

In Table 6.5, the results from the numerical tests are displayed with the experimental tests and calculations performed by Haande and Thunberg(3). The disparity between

the calculated and numerical outcomes is less than 5% in all instances. Three of the four tests were above this margin, while one fell below. In comparison to the experimental values, the numerical values are marginally under 10%, and predominantly lower. Given that the timber used for this thesis was the same as that in Thunberg and Haande's study, the density measurements conducted in this thesis are also applicable to these experimental results. Although data for the exact specimen is unavailable, almost all the timber specimens exhibited a higher density than the mean. Consequently, it can be expected that these tests would yield a higher load. To sum up, the numerical model estimated the load accurately.

Test	Haande and Thunberg	Numerical result	Predicted	Numerical vs experimental	Numerical vs predicted
S_8.0_200_B	226 kN	219kN	209kN	-3%	5%
Pe_7.0_160_B	177 kN	167kN	171kN	-6%	-2%
Pe_8.2_160_B	189 kN	169kN	178kN	-11%	-5%
Pe_8.0_200_B	213 kN	177kN	178kN	-17%	-1%

Table 6.5: Numerical results initial study

7. Final remarks

7.1 Conclusion

The objective of this thesis was to investigate the proposal by Aloisio et al.(7), evaluating its alignment with both experimental and numerical tests, and to identify contributing factors to the increase and decrease of buckling capacity.

- The outcomes of both the numerical and experimental tests affirm the proposal with respect to the buckling mode. For the 8 mm screws, the buckling load closely matched the mathematical model. The 10 mm screws, however, demonstrated a significantly lower buckling load. Thus, buckling mode is affirmed, but there remain some uncertainties regarding the calculated loads.
- Upon researching which factors contribute most to the buckling capacity, it became clear that both the density and the geometrical imperfection a_g need to be more accurately modeled. The a_g value seemed to fit best at 0.3. However, as the impact of density emerged as a significant contributor, this may require further adjustment, given the remaining uncertainties. The model for calculating C_h based on density needs refinement, as the results indicate that the contribution is much larger than the current formula suggests.

7.2 Further Work

- The need for more data incorporating different dimensions is evident in order to verify whether or not the calculation model of Aloisio et al.(7) is applicable to all dimensions.
- The geometrical imperfection a_g requires more precise modeling.By a higher number of tests from different manufactures as the screw it self could affect this.
- The model for calculating C_h demands thorough investigation and potential adjustment or a new formula.

Bibliography

[1] Li Y. Wood-Polymer Composites. InTech; 2011. Available from: https://www.researchgate.net/publication/221915965_Wood-Polymer_Composites.

[2] Müller U, Gindl W, Teischinger A. EFFECTS OF CELL ANATOMY ON THE PLASTIC AND ELASTIC BEHAVIOUR OF DIFFERENT WOOD SPECIES LOADED PERPENDICULAR TO GRAIN; 2003. Available from: https://brill.com/view/journals/iawa/24/2/article-p117_2.xml?language=en.

[3] Hånde EA, Thunberg KR. An Assessment of the Design Model for Glulam Members subjected to Compression Perpendicular to the Grain with Reinforcement; 2022. Available from: https://hdl.handle.net/11250/3033400.

[4] Ringhofer A. Axially Loaded Self-Tapping Screws in Solid Timber and Laminated Timber Products; 2017. Available from: https://openlib.tugraz.at/download.php?id=5dd3c9c9585aa&location=browse.

[5] Weißbach W. Werkstoffkunde; 2015.

[6] i Bejkta, Blaß HJ. INTERNATIONAL COUNCIL FOR RESEARCH AND INNOVATION IN BUILDING AND CONSTRUCTION WORKING COMMISSION W18-TIMBER STRUCTURES SELF-TAPPING SCREWS AS REINFORCEMENTS IN BEAM SUPPORTS I Bejtka; 2006. Available from: https://publikationen.bibliothek.kit.edu/1000007094/676237.

[7] Aloisio A, Santis YD, Pelliciari M, Rosso MM, Fragiacomo M, Tomasi R. https://www.sciencedirect.com/science/article/pii/S0950061823009388. Construction and Building Materials. 2023 5;379.

[8] Santis YD, Sciomenta M, Spera L, Rinaldi V, Fragiacomo M, Bedon C. Effect of Interlayer and Inclined Screw Arrangements on the Load-Bearing Capacity of Timber-Concrete Composite Connections. Buildings. 2022 12;12. Available from: https://www.mdpi.com/2075-5309/12/12/2076.

[9] Lennartz AN, Hamilton MD, Herrmann NP, Wescott DJ, Weaver R. ASSESS-

ING PATTERNS OF MOISTURE CONTENT IN DECOMPOSING, DESICCATED, AND MUMMIFIED TISSUE: A BASELINE STUDY Committee Members; 2018. Available from: https://digital.library.txstate.edu/bitstream/handle/10877/7456/LENNARTZ-THESIS-2018.pdf?sequence=1.

[10] Høibø OA, Vestøl GI. 1 Vannopptak og svelling. 1 Vannopptak og svelling. 2021Available from: https://www.youtube.com/watch?v=dVx8En8ol7E.

[11] Tomasi R, Aloisio A, Hånde EA, Thunberg KR, Ussher E. Experimental investigation on screw reinforcement of timber members under compression perpendicular to the grain. Engineering Structures. 2023 1;275. Available from: https://www.sciencedirect.com/science/article/pii/S0141029622012391.

[12] Bazli M, Heitzmann M, Ashrafi H. Long-span timber flooring systems: A systematic review from structural performance and design considerations to constructability and sustainability aspects. Elsevier Ltd; 2022. Available from: https://www.sciencedirect.com/science/article/abs/pii/S2352710221018398.

[13] Mascia NT, Lahr FAR. Remarks on orthotropic elastic models applied to wood. Materials Research. 2006;9:301-10. Available from: https://www.researchgate.net/publication/250029609_Remarks_on_orthotropic_elastic_models_applied_to_wood.

[14] Bjetka I. I. Bejtka Verstärkung von Bauteilen aus Holz mit Vollgewindeschrauben; 2005. Available from: https://publikationen.bibliothek.kit.edu/1000003354.

[15] Nilsson K. Avdelningen för Konstruktionsteknik Lunds Tekniska Högskola, Lund Universitet skruvarmering som förstärkning i trä vid belastning vinkelrätt fiberriktningen-en förssöksstudie; 2002. Available from: https://lup.lub.lu.se/luur/download?func=downloadFile&recordOId=3172244&fileOId=4462079.

[16] Kollmann FFP, Côté WA. Principles of Wood Science and Technology. 1st ed. Springer Berlin Heidelberg; 1968.

[17] Fortino S, Hradil P, Salminen LI, Magistris FD. A 3D micromechanical study of deformation curves and cell wall stresses in wood under transverse loading. A 3D micromechanical study of deformation curves and cell wall stresses in wood under transverse loading. 2015. Available from: https://link.springer.com/article/10.1007/s10853-014-8608-2.

[18] Forening NL. LIMTREBOKA; 2015. Available from: https://www.moelven.com/globalassets/moelven-limtre/limtreboka_2015_el2.pdf.

[19] Abaqus. Dassault Systems Simulia; 2017. Available from: https://www.3ds.com/products-services/simulia/products/abaqus/.

[20] Tekkaya AE, Soyarslan C. Finite Element Method. Springer Berlin Heidelberg; 2014. Available from: https://link.springer.com/referenceworkentry/10.1007/978-3-642-20617-7_16699.

[21] Grytting H, Sæle ED. Aksial-og tverrbelastede gjengestenger i trekonstruksjoner. 2015. Available from: https://ntnuopen.ntnu.no/ntnu-xmlui/handle/11250/2359022.

[22] Corp DSS. ABAQUS Analysis User's Manual, 18.2.6 Anisotropic yield/creep;. Available from: https://classes.engineering.wustl.edu/2009/spring/mase5513/abaqus/docs/v6.6/books/usb/default.htm?startat=pt05ch18s02abm20.html.

[23] Ellobody E. Finite Element Analysis and Design of Steel and Steelconcrete Composite Bridges. Elsevier; 2023. Available from: https://www.elsevier.com/books/finite-element-analysis-and-design-of-steel-and-steel-concrete-composite-bridge
ellobody/978-0-12-417247-0.

[24] Computers I, Structures. Eigenvalue vs. Nonlinear buckling analysis; 2019. Available from: https://wiki.csiamerica.com/display/kb/Eigenvalue+vs.+Nonlinear+buckling+analysis.

[25] Corp DSS. Eigenvalue buckling prediction;. Available from: https://classes.engineering.wustl.edu/2009/spring/mase5513/abaqus/docs/v6.6/books/usb/default.htm?startat=pt03ch06s02at02.html.

[26] Almar-Næss A. Herding (metallurgi). SNLno. 2023Available from: https://snl.no/herding_-_metallurgi.

[27] HT-plus-ETA-19_0553; 2020.

[28] Avez C, Descamps T, Serrano E, Léoskool L. Finite element modelling of inclined screwed timber to timber connections with a large gap between the elements. European Journal of Wood and Wood Products. 2016 5;74:467-71. Available from: https://link.springer.com/article/10.1007/s00107-015-1002-1.

[29] Bedon C, Fragiacomo M. Numerical analysis of timber-to-timber joints and composite beams with inclined self-tapping screws. Composite Structures. 2019 1;207:13-28. Available from: https://www.sciencedirect.com/science/article/abs/pii/S0263822318316970.

[30] Hardeng A. The baring capacity of locally loaded beams ans sills for compression perpendicular to the grain. The baring capacity of locally loaded beams ans sills for compression perpendicular to the grain. 2011. Available from: https://nmbu.brage.unit.no/nmbu-xmlui/handle/11250/188736.

[31] Kučera B. Skandinaviske normer for testing av små feilfrie prøver av heltre. 1992:21-6.

Appendix A. Result extracting

```
# -*- coding: utf-8 -*-
"""
Created on Thu Feb 16 10:17:27 2023

@author: Martin Steimler
"""
import pandas as pd
import matplotlib.pyplot as plt
import numpy as np
from shapely.geometry import LineString
import os

def F_estimated (Fest_2):
        F_est = Fest_2
        Fest04 = F_est*0.4
        Fest01 = F_est/10

        # find the index of the row that has the closest value to Fest01 and Fest04
        idx_fest01 = df['Standard force'].sub(Fest01).abs().idxmin()
        idx_fest04 = df['Standard force'].sub(Fest04).abs().idxmin()

        # get the screw-def values for Fest01 and Fest04
        screw_def_fest01 = df.loc[idx_fest01, 'screw-def']
        screw_def_fest04 = df.loc[idx_fest04, 'screw-def']
```

```
# use screw-def, Fest01, and Fest04 to find the gradient
gradient = (screw_def_fest04 - screw_def_fest01) / (Fest04 - Fest01)

# create a scatter plot of 'screw-def' and 'Standard force'
plt.scatter(df['screw-def'], df['Standard force'], color='black', s=5)
plt.xlabel('Screw-Def')
plt.ylabel('Standard Force')
plt.title('Screw-Def vs Standard Force')


# plot Fest01 and Fest04 as green dots
plt.scatter([screw_def_fest01, screw_def_fest04], [Fest01, Fest04], color='green')

# plot the line in red
y_vals = [0, 1.3*Fest04*2]
x_vals = [screw_def_fest01, screw_def_fest01 + gradient*(1.3*Fest04 - Fest01)*2]
plt.plot(x_vals, y_vals, '--r', linewidth=1, label='gradient')


# plot the copy of the gradient line in black, moved the length of screw-def/100
length_screw = Length_screw  # define the length of screw-def
y_vals = [0, 1.3*Fest04*4]
x_vals = [screw_def_fest01+length_screw/100, screw_def_fest01 + gradient*(1.3*Fest04 - Fest01)*4+length_screw/100]
plt.plot(x_vals, y_vals, '--r', linewidth=1, label='gradient')
```

```
# find the starting point of the second red line
idx_intersection = (df['screw-def'] - screw_def_fest01 - length_screw/100) / gradient
idx_intersection = idx_intersection[idx_intersection.between(Fest01, Fest04)].index.min()

# get the y-value of the intersection point
y_intersection = df.loc[idx_intersection, 'Standard force']
plt.scatter(df.loc[idx_intersection, 'screw-def'], y_intersection, color='green')


first_line = LineString(np.column_stack((df['screw-def'], df['Standard force'])))
second_line = LineString(np.column_stack((x_vals, y_vals)))
intersection = first_line.intersection(second_line)

#finds intersection
if intersection.geom_type == 'MultiPoint':
    plt.plot(*LineString(intersection).xy, 'o')
elif intersection.geom_type == 'Point':
    plt.plot(*intersection.xy, 'o')

fig.set_size_inches(8, 6)
filename = "Results"
filename += '.png'

plt.savefig(filename)
#doc.add_picture(filename, width=docx.shared.Inches(6))
```

```
        plt.show()
        #print(intersection.xy)

        #assign value Fest_2
        Fest_3 = intersection.xy[1][0]


        #doc.add_paragraph('The value of Fest is {} for a screw length of {} mm.'.format(Fest_3, Length_screw))
        return Fest_3

Length_screw = 120

folder_path = "C:/Users/Martin/Documents/Master/All tests/8x120"

# create an empty list to store the filenames
filenames = []

# loop through all TXT files in the folder and append their names to the list
for filename in os.listdir(folder_path):
    if filename.endswith(".TXT"):
        filenames.append(filename)

# convert the list of filenames into a DataFrame
df_filenames = pd.DataFrame(filenames, columns=["Filename"])
```

```
# print the DataFrame
#print(df_filenames)
a=0
# loop through all TXT files in the folder
for Filename in df_filenames.Filename:

        print(Filename)

        a += 1
        print(a)
        #print(folder_path)
        #print(file_path)
        file_path = folder_path + "/" + Filename
        #file_path = os.path.join(folder_path, filename)
        # call the script with the file path as an argument
        #print(file_path)
        #os.system(f"python C:/Users/Martin/Documents/Master/All tests/8x120/Fest,i_2.py {file_path} {F_est} {Length_screw}")
#file_path = "NS-ISO_6891_01_forste_runde_M4.3-00-#4-8x200_1.TXT"

# define the file path and column delimiter
        F_est = 15615.49

        Fest04 = F_est*0.4
        Fest01 = F_est/10
```

```
#doc = docx.Document()

delimiter = ';'

# read the data into a Pandas DataFrame
df = pd.read_csv(file_path, delimiter=delimiter)

# drop the first row of the DataFrame
df = df.drop([0])

# remove the 'mm' unit label from the 'Deformasjon' column header
df = df.rename(columns={'Deformasjon': 'Deformasjon [mm]'})

# convert the 'Deformasjon [mm]' column to float
df['Deformasjon [mm]'] = df['Deformasjon [mm]'].astype(float)

# convert 'Heiden_Blue' and 'Heiden_Green' columns to float
df['Heiden_Blue'] = df['Heiden_Blue'].astype(float)
df['Heiden_Green'] = df['Heiden_Green'].astype(float)

# add new column screw-def
df['screw-def'] = df['Deformasjon [mm]'] - ((df['Heiden_Blue'] + df['Heiden_Green']) / 2)

# convert 'Standard force' column to numeric values
df['Standard force'] = pd.to_numeric(df['Standard force'], errors='coerce')
```

```
# fill NaN values with -9999
df['Standard force'] = df['Standard force'].fillna(-9999)

# find the first Fest04 value within 50 and delete all rows before it
index_fest04 = df[df['Standard force'].between(Fest04-50, Fest04+50)].index.min()
if index_fest04 is not None:
    df = df.iloc[index_fest04-1:]
#print(df)
#gg = df
# Find the index of the row where the first occurrence of fest01 happens

idx_Fest01 = df[df['Standard force'].between(Fest01 - 50, Fest01 + 50)].index.min()
if np.isnan(idx_Fest01):
    idx_Fest01 = df[df['Standard force'].between(Fest01 - 200, Fest01 + 200)].index.min()

# Delete all rows before the row with index idx_fest01
df = df.loc[idx_Fest01:]

# find the index of the last occurrence of 'Fest0.1'
last_fest01_index = df[df['Standard force'] == 'Fest0.1'].last_valid_index()

# drop all rows with 'Fest0.1' except the last occurrence
if last_fest01_index is not None:
    df = df.drop(df.index[df.index < last_fest01_index])
```

```
# find the index of the row that has the closest value to Fest01 and Fest04
idx_fest01 = df['Standard force'].sub(Fest01).abs().idxmin()
idx_fest04 = df['Standard force'].sub(Fest04).abs().idxmin()

# get the screw-def values for Fest01 and Fest04
screw_def_fest01 = df.loc[idx_fest01, 'screw-def']
screw_def_fest04 = df.loc[idx_fest04, 'screw-def']

# use screw-def, Fest01, and Fest04 to find the gradient
gradient = (screw_def_fest04 - screw_def_fest01) / (Fest04 - Fest01)

# create a scatter plot of 'screw-def' and 'Standard force'
plt.scatter(df['screw-def'], df['Standard force'], color='black', s=5)
plt.xlabel('Screw-Def')
plt.ylabel('Standard Force')
plt.title('Screw-Def vs Standard Force')

# plot Fest01 and Fest04 as green dots
plt.scatter([screw_def_fest01, screw_def_fest04], [Fest01, Fest04], color='green')

# plot the line in red
y_vals = [0, 1.3*Fest04*2]
x_vals = [screw_def_fest01, screw_def_fest01 + gradient*(1.3*Fest04 - Fest01)*2]
plt.plot(x_vals, y_vals, '--r', linewidth=1, label='gradient')
```

```
# plot the copy of the gradient line in black, moved the length of screw-def/100
length_screw = Length_screw  # define the length of screw-def
y_vals = [0, 1.3*Fest04*4]
x_vals = [screw_def_fest01+length_screw/100, screw_def_fest01 + gradient*(1.3*Fest04 - Fest01)*4+length_screw/100]
plt.plot(x_vals, y_vals, '--r', linewidth=1, label='gradient')

# find the starting point of the second red line
idx_intersection = (df['screw-def'] - screw_def_fest01 - length_screw/100) / gradient
idx_intersection = idx_intersection[idx_intersection.between(Fest01, Fest04)].index.min()

# get the y-value of the intersection point
y_intersection = df.loc[idx_intersection, 'Standard force']
plt.scatter(df.loc[idx_intersection, 'screw-def'], y_intersection, color='green')

first_line = LineString(np.column_stack((df['screw-def'], df['Standard force'])))
second_line = LineString(np.column_stack((x_vals, y_vals)))
intersection = first_line.intersection(second_line)

#finds intersection
if intersection.geom_type == 'MultiPoint':
    plt.plot(*LineString(intersection).xy, 'o')
elif intersection.geom_type == 'Point':
    plt.plot(*intersection.xy, 'o')
```

```
fig = plt.gcf()

# modify the figure's properties
fig.set_size_inches(8, 6)
filename = "Results"
filename += '.png'

plt.savefig(filename)
#doc.add_picture(filename, width=docx.shared.Inches(6))

plt.show()

#print(intersection.xy)
Fest = 1
#assign value Fest_2
Fest_2 = intersection.xy[1][0]
if abs((Fest_2-F_est))/F_est <= 0.05:
    #doc.add_paragraph('The value of Fest is {}.'.format(Fest_2))
    Fest = Fest_2
    print((Fest))

else:
    Fest_3 =  F_estimated(Fest_2)
    if abs((Fest_3-Fest_2))/F_est <= 0.05:
        #doc.add_paragraph('The value of Fest is {}.'.format(Fest_2))
```

```
        Fest = Fest_3
        print((Fest))

    if not abs((Fest_3-Fest_2))/F_est <= 0.05:
        Fest_4 = F_estimated(Fest_3)
        if abs((Fest_4-Fest_3))/F_est <= 0.05:
            #doc.add_paragraph('The value of Fest is {}.'.format(Fest_2))
            Fest = Fest_4
            print((Fest))
df =""
```